

**Early-warning indicator based on autoregressive moving-average models:
Critical Transitions and the Atlantic Meridional Overturning Circulation**

Marie Rodal,^{1, a)} Sebastian Krumscheid,² Gaurav Madan,³ Joseph Henry LaCasce,³ and
Nikki Vercauteren^{3, b)}

¹⁾*FB Mathematik und Informatik, Freie Universität Berlin, Arnimallee 6,
14195 Berlin, Germany*

²⁾*Department of Mathematics, RWTH Aachen, Templergraben 55, 52062 Aachen,
Germany*

³⁾*Section for Meteorology and Oceanography, Department of Geosciences,
University of Oslo, Blindernveien 31, Kristine Bonnevis hus, 0371 Oslo,
Norway*

(Dated: 3 March 2022)

A statistical indicator for dynamic stability based on autoregressive moving-average, ARMA(p,q), models is used to gauge the stability and hence predict approaching tipping points of simulation data from a reduced 5-box model of the North-Atlantic Meridional Overturning Circulation (AMOC) exposed to a time dependent hosing function. The hosing function simulates the influx of fresh water due to the melting of the Greenland ice sheet and increased precipitation in the North Atlantic. We study the indicator's ability to assess the stability of a time series subject to different types of tipping, including bifurcation-induced and rate-induced tipping, and show that the indicator is indeed able to identify the different types of induced instability. In the process we extend the underlying models from an ARMA(p,q) process to an ARIMA(p,q) (autoregressive *integrated* moving-average) process, which through the proper application of differencing converts a formerly non-stationary process into a stationary one, further extending the regime of validity of the statistical method. In addition, we apply the indicator to simulation data from the Earth systems model CESM2, to assess how the indicator responds to more realistic time series data.

^{a)}marie.rodal@fu-berlin.de

^{b)}nikki.vercauteren@geo.uio.no

I. INTRODUCTION

Tipping points, or critical transitions, are sudden, drastic changes in a system resulting from minor changes in input. The study of tipping points is of particular interest to climate scientists and ecologists, as several theoretical studies predict such tipping for an assortment of climatic and ecological systems, and observations also indicate that abrupt changes are, indeed, common in nature.

Ashwin *et al.*¹ classified tipping points according to the causing mechanism, yielding three classes of tipping points, namely rate-induced, bifurcation-induced, and noise-induced tipping, also known as R-, B-, and N-tipping, respectively.

Of these three, rate-induced tipping is certainly the least studied, however as demonstrated by Scheffer *et al.*², Wieczorek *et al.*³ and more recently O’Keeffe and Wieczorek⁴, it is an important tipping mechanism that cannot be explained through classical bifurcation theory. Rate-induced tipping occurs when the system is unable to track a continuously available quasi-stable state, due to the system parameters changing too quickly. Thus, the system might shift to another available equilibrium state without crossing a bifurcation boundary. There are a few methods available for estimating what exactly "too quickly" means, see Wieczorek and Perryman⁵, Ashwin, Perryman, and Wieczorek⁶, Vanselow, Wieczorek, and Feudel⁷ and O’Keeffe and Wieczorek⁴, but they depend strongly on the time-dependent parameter function; in particular its asymptotic properties. Finding generalizable methods for determining the rate of parameter drift that induces tipping, will be of great interest going forward. Another issue of great practical importance is the question of how to predict such tipping points, in particular if classical methods for stability analysis also remain valid in the regime of rapid parameter change.

Ritchie and Sieber⁸ showed that for rate-induced tipping, the most commonly used early-warning indicators, increase in variance and increase in autocorrelation, occur not when the equilibrium drift is fastest but with a delay. This suggests that these indicators might not be able to detect tipping before it has already occurred, although their analysis does give indication that the theory behind these indicators, the so-called "critical slowing down", would still hold for rate-induced tipping.

In this paper, we wish to study an indicator for dynamic stability, from now on referred to as the Υ *indicator*, initially proposed by Faranda *et al.*⁹. The Υ *indicator* uses ARMA(p,q)

models to estimate how close a system is to an equilibrium, and is based on the observation that a system very close to an equilibrium will resemble an ARMA(1,0) process. The indicator was later applied to atmospheric boundary layer data by Nevo *et al.*¹⁰, Kaiser *et al.*¹¹ and Faranda and DeFrance¹². They successfully demonstrated the indicator's ability to both gauge the stability of a time series and predict tipping points. However, the indicator requires some additional testing, in particular as it relates to rate-induced tipping, which thus far has not been explored. It should be noted that several different early warning indicators based on ARMA models have been proposed. In fact, in Faranda, Dubrulle, and Pons¹³ the authors propose the sum of the p and q orders of the model, as well as the sum of the model coefficients as potential indicators. The sum of the order parameters then gives an estimate for the memory lag of the process, while the sum of the model coefficients gives the persistence of this memory lag.

To further test the indicator, we have chosen the global oceanic 3-box model studied by Alkhayuon *et al.*¹⁴, which in turn is based upon the 5-box model of Wood *et al.*¹⁵. The model represents a simplified Atlantic Meridional Overturning Circulation (AMOC), which transports warm surface water from the tropics to North America and Europe, resulting in a milder climate in these regions than what would otherwise be expected. Since the current is density driven, a large influx of freshwater due to the melting of land ice or increased precipitation in the North Atlantic, would be expected to result in a reduction in the AMOC flow strength. The question of whether the AMOC could undergo a sudden transition from a high flow strength state (the "on" state) to a state with weak or no overturning (the "off" state), is still debated. The latest assessment report of the International Panel for Climate Change (IPCC AR6) concludes that the AMOC strength will very likely decline in the future, but states with medium confidence that an abrupt collapse will not occur in the next century¹⁶. Simple box models, like the one presented in this paper, show bi-stability, while more realistic models like the global atmosphere-ocean general circulation models (AOGCMs) are largely mono-stable, implying that they do not exhibit the abrupt transition to an "off"-state so characteristic of the simpler models. However, there is limited evidence that the more complex models may be too stable (Weijer *et al.*¹⁷, Hofmann and Rahmsdorf¹⁸ and Liu *et al.*¹⁹), in particular that they mis-represent the direction of AMOC-induced freshwater transport across the southern boundary of the Atlantic (Liu *et al.*¹⁹, Huisman *et al.*²⁰, Liu, Liu, and Brady²¹, Hawkins *et al.*²²). Liu *et al.*¹⁹ demon-

strated that by introducing a flux-correction term into the National Center for Atmospheric Research (NCAR) Community Climate System Model version 3 (CCSM3), they could make the formerly mono-stable system bi-stable.

In addition, it has been suggested that paleoclimate data is consistent with abrupt changes in the surface temperature in the North Atlantic region in the past, as might be expected with a collapse of the AMOC. Boers²³ applied a statistical early warning indicator on Earth System Model (ESM) outputs, and found significant early-warning signals in eight independent AMOC indices. This was interpreted as a sign that the AMOC is not only a bistable system, but one approaching a critical transition.

Previously, the potential collapse of the AMOC has largely been attributed to the crossing of a bifurcation boundary in the bi-stable system. However, more recent analysis, see in particular Lohman and Ditlevsen²⁴, demonstrate the possibility of tipping before the bifurcation boundary is reached through the mechanism of rate-induced tipping. In addition, Lohman and Ditlevsen²⁴ demonstrate that due to the chaotic nature of complex systems a well-defined critical rate, i.e., the rate of parameter change at which the system tips, cannot be obtained, which in turn severely limits our ability to predict the long-term behavior of the system. They conclude that due to this added level of uncertainty, it is possible that the safe operating space with regard to future emissions of CO₂ might be smaller than previously thought. This suggests that proper evaluation of the probability of rate-induced tipping in the different tipping elements of the Earth System is of utmost importance in assessing the likelihood of dramatic future changes.

Regardless of whether the AMOC in actuality is bi-stable or mono-stable, the reduced 5-box model of Alkhayon *et al.*¹⁴ is the perfect test case for the Υ *indicator* as it exhibits both bifurcation-induced and rate-induced tipping, provided a time dependent hosing function is applied. The hosing function represents the influx of fresh water into the ocean due to increased precipitation and melting of land and sea ice in the North Atlantic region. Alkhayon *et al.*¹⁴ provide an extensive analysis of the tipping mechanisms present in the model. Armed with such a well studied theoretical model, we will be able to systematically study the indicator's ability to not only predict bifurcation-induced and noise-induced, but also rate-induced tipping.

We will also apply the Υ *indicator* to monthly ocean data from two separate simulations

conducted under the Coupled Model Intercomparison Project (CMIP6), with the Community Earth System Model (CESM2)²⁵.

Finally, we will assess the indicator’s ability to deal with colored noise, something that is known to cause issues for other early warning indicators, like the increase in variance and auto-correlation.

II. THE Υ -INDICATOR FOR EARLY-WARNING SIGNALS

In what follows, we will briefly outline the method used to determine the stability of the time series data. Further details can be found in Faranda *et al.*⁹, Faranda and Defrance¹², Nevo *et al.*¹⁰ and Kaiser *et al.*¹¹

The method uses that even for a complex system, the dynamics near a metastable state resembles that of a stochastic spring, in which the discretized system becomes an ARMA(1,0) process. Here, ARMA denotes the space of autoregressive moving-average models, with the numbers in parentheses denoting the order of the model. A time series $x(t)$, $t \in \mathbf{Z}$, is an ARMA(p,q) process if it is stationary and can be written as

$$x(t) = \nu + \sum_{i=1}^p \phi_i x_{t-i} + \sum_{j=1}^q \theta_j w_{t-j} + w_t \quad (1)$$

with constant ν , coefficients ϕ_i , θ_j and $\{w_t\}$ being white noise with positive variance σ^2 . Intuitively, the variables p and q say something about the memory lag of the process, while the prefactors ϕ_i and θ_j relate to the persistence of said memory lag. We would expect that the higher the values for q and p the longer the system, once perturbed from its equilibrium state, would need to return to equilibrium. It is this intuitive notion that the statistical indicator denoted Υ takes advantage of. By fitting equation (1) repeatedly to a time series data set for varying values of p and q , one can, through application of an appropriate information criterion, obtain the values of p and q that best represent the time series data. For this purpose, we choose the Bayesian information criterion, BIC, which has to be minimized. It is defined as

$$\text{BIC} = -2 \ln L(\hat{\beta}) + \ln(\tau)(p + q - 1) \quad (2)$$

where $L(\hat{\beta})$ denotes the associated likelihood function evaluated at the maximum likelihood estimator $\hat{\beta}$. The second term in equation (2) punishes complex models with high p and q

The Υ *indicator* for Early Warning

values, and is the reason why we prefer to use the BIC over the perhaps more familiar AIC (Akaike Information Criterion).

Finally, the stability indicator is defined as

$$\Upsilon(p, q; \tau) = 1 - \exp\left(\frac{-|\text{BIC}(p, q) - \text{BIC}(1, 0)|}{\tau}\right) \quad (3)$$

The Υ -indicator takes on values between 0 and 1, where lower values imply a higher degree of stability. The intuition behind using the difference in BIC values between the chosen "best" model and a base model (in our case the AR(1) model) is that this quantity quantifies just how much better the model with the lower BIC value is compared to the other. The significance threshold is $|\Delta\text{BIC}| > 2$, and these values can be directly related to the Bayes Factor, see Preacher and Merkle²⁶, which is another way of quantifying the likelihood of one model over another.

Furthermore, we define the *order*, $\mathcal{O}(\tau)$, and *persistence*, $\mathcal{R}(\tau)$, of an ARMA(p, q) process as

$$\mathcal{O}(\tau) = p + q \quad (4)$$

$$\mathcal{R}(\tau) = \sum_{i=1}^p |\phi_i| + \sum_{i=1}^q |\theta_j| \quad (5)$$

where ϕ_i and θ_j denote the autoregressive and moving-average coefficients, respectively. While the order relates to the memory lag of the process, the persistence relates to the *persistence* of said memory lag, hence the name. When approaching a tipping point, one would expect one out of two things to happen: either both the persistence and the order diverges, due to the increased memory of the process, or the order remains constant, and the persistence approaches this value, indicating a loss of stationarity. The latter alternative corresponds to a case in which the potential landscape of the system does not change considerably when approaching the transition, see Faranda, Dubrulle, and Pons¹³.

To apply the method to a time series data set, one first has to ensure stationarity of the data. This can be done in two ways, depending on the nature of the time series. In some cases, it is sufficient to split the time series into small enough intervals, so that within each interval the time series is approximately stationary. To check for stationarity one runs a Kwiatkowski–Phillips–Schmidt–Shin (KPSS) tests on the intervals. This way, one also obtains an upper bound on the length of the intervals. The other option is to not assume

stationarity from the outset, and instead allow for application of a differencing routine to the separate intervals, achieving stationarity that way. In that case, a KPSS test is run on each interval, and if the interval is found to not be stationary, differencing is applied. This process is then repeated until stationarity is achieved. The KPSS test is to be preferred over the unit root test due to the danger of over-differencing (Hyndman and Khandakar²⁷). As we wish to study rate induced tipping phenomena, which yields highly non-stationary time series even for very small interval lengths, the latter method is to be preferred.

Provided one can make the time series intervals stationary, one can fit ARMA(p,q) models to the intervals, and through the Υ indicator obtain an estimate for how close any given interval is to an equilibrium state.

It is clear that the method is strongly dependent upon the size of the intervals, which we will refer to as the window length, denoted τ . This is not only due to the inclusion of the $1/\tau$ factor in the exponential, but also due to the inherent τ -dependence of $\text{BIC}(p, q)$ and $\text{BIC}(1, 0)$. In fact, the rationale for including the $1/\tau$ factor in the definition of Υ is to attempt to remove or reduce this dependence. From equation (2) one might conclude that the correct scaling would be $1/\ln(\tau)$, as opposed to $1/\tau$. However, we do not only want to remove the dependence on τ , but also include the significance threshold for ΔBIC , such that the Υ value of any point where ΔBIC is below 2 is suppressed relative to other points.

To determine the best fit, we use the `auto.arima` function found in the FORECAST R package, setting BIC as the information criterion used for model selection. Since we will not assume stationarity of the time series, `auto.arima` first determines the correct differencing order before continuing with the fitting procedure; the details of said procedure can be found in Hyndman and Khandakar²⁷. As the purpose of `auto.arima` is to yield the best forecast model (remember that ARIMA-modelling is primarily used for time series forecasting), the fitted parameter values are subject to some additional constraints, in particular it will not return a model whose roots are within the unit circle. In fact, `auto.arima` will reject any model with roots smaller than 1.001, to ensure that the solution is numerically well-behaved. This implies that it is possible to have time series for which the BIC value of the AR(1) model is smaller than the corresponding value for the chosen ARMA(p,q) model. In these cases, it is unclear how to determine the 'distance' between the states, and one would have

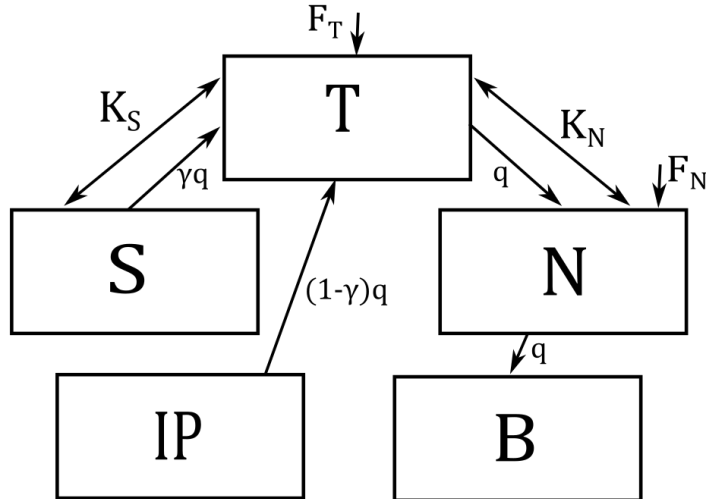


FIG. 1: Sketch of the 3-box model for the Atlantic Meridional Overturning Circulation (AMOC). Adapted from Alkhayuon *et al.*¹⁴.

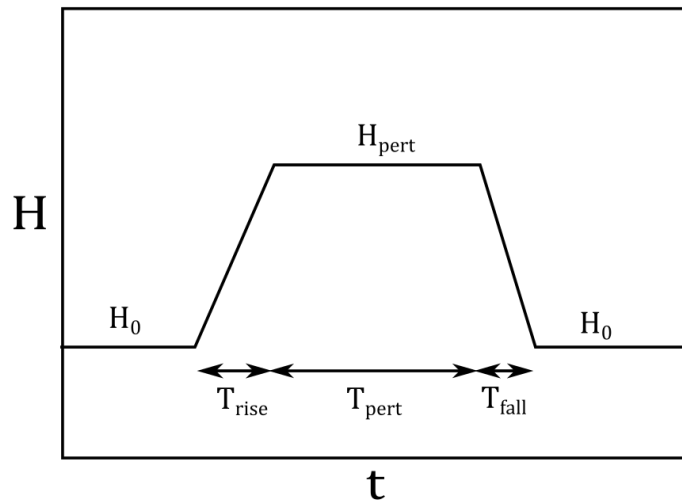


FIG. 2: Schematic illustration of the piece-wise linear hosing function used to simulate the influx of fresh water. Adapted from Alkhayuon *et al.*¹⁴.

to resort to looking at other properties of the process, such as the order or persistence values, to get an idea about the stability properties of the system.

Finally, we note that auto.arima is guaranteed to return a valid model because at least one of the models will be accepted, namely the ARMA(0,0) model, which is just white noise possibly with a drift. Hence, it is conceivable that this model will be the most common

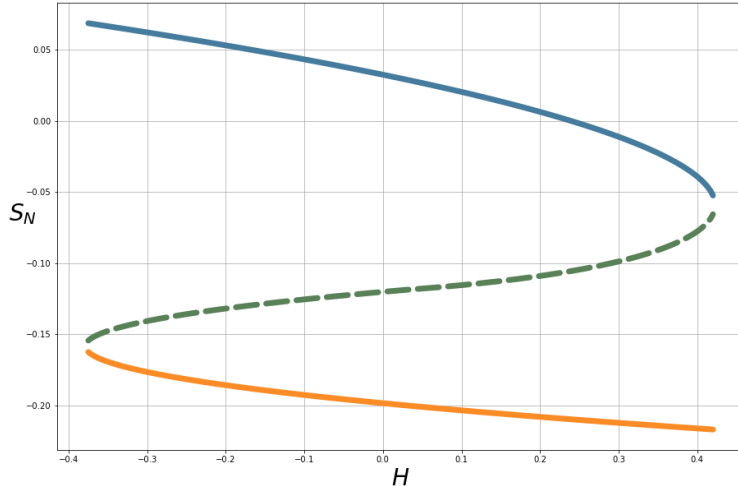


FIG. 3: Bifurcation diagram for S_N , for the 3-box model of the AMOC. The dashed line denotes the unstable equilibrium branch.

model, given the algorithmic procedure.

III. APPLICATION TO THE GLOBAL OCEANIC 3-BOX MODEL

To determine the validity of the Υ -indicator as a measure of stability, as well as its ability to predict tipping points, we start by applying the method to the global oceanic 3-box model discussed by Alkhayuon *et al.*¹⁴. The 3-box model of Alkhayuon *et al.* is a simplification of the 5-box model of Wood *et al.*¹⁵ in which the salinity of the Southern Ocean (S) and the Bottom waters (B) is assumed to be approximately constant. The model thus consists of 5 separate boxes, of which only 3 boxes, namely the North Atlantic (N), Tropical Atlantic (T) and Indo-Pacific (IP) boxes have varying salinities S . A schematic illustration of the model is shown in Figure 1. See Alkhayuon *et al.* or Wood *et al.* for a detailed exposition of the box model. We note that the parameters of the box model are tuned using the full complexity FAMOUS AOGCM model, with varying levels of CO_2 . The parameters used in this paper are for the case $2\times\text{CO}_2$ as compared to pre-industrial times.

We denote salinity by S_i , the volume by V_i and the fluxes by F_i , where $i \in [N, T, S, IP, B]$ denotes the respective boxes.

The Υ indicator for Early Warning

Let q denote the AMOC flow defined by

$$q = \lambda \left[\alpha(T_S - T_0) + \frac{\beta}{100}(S_N - S_S) \right] \quad (6)$$

The model approximates a buoyancy-driven flow, with a transport proportional to the density difference between the boxes, assuming a linearized equation of state. The evolution equations for the salinities S_N and S_T are

$$\frac{V_N}{Y} \frac{dS_N}{dt} = q(S_T - S_N) + K_N(S_T - S_N) - 100F_N S_0 \quad (7)$$

$$\frac{V_T}{Y} \frac{dS_T}{dt} = q[\gamma S_S + (1 - \gamma)S_{IP} - S_T] + K_S(S_S - S_T) + K_N(S_N - S_T) - 100F_T S_0 \quad (8)$$

for $q \geq 0$, and

$$\frac{V_N}{Y} \frac{dS_N}{dt} = |q|(S_B - S_N) + K_N(S_T - S_N) - 100F_N S_0 \quad (9)$$

$$\frac{V_T}{Y} \frac{dS_T}{dt} = |q|(S_N - S_T) + K_S(S_S - S_T) + K_N(S_N - S_T) - 100F_T S_0 \quad (10)$$

for $q < 0$, where S_B and S_S are regarded as fixed parameters and $Y = 3.15 \times 10^7$, which converts the time unit from seconds to years. S_0 is a reference salinity, and K_i are coefficients associated with the gyre strengths. We note that all the salinity values are given as perturbations from a background state, see Appendix A of Alkhayoun *et al.* for details on the transformation.

The values of the assorted parameters can be found in Table 1 and Table 2.

Figure 3 shows the bifurcation diagram for S_N ; for S_T we refer to Alkhayoun *et al.* The diagram clearly shows that this is a bi-stable system with two stable equilibrium branches connected by an unstable branch. The diagram as it stands is a little deceptive, as it gives the impression that the upper equilibrium branch is destroyed due to a saddle node bifurcation, while in fact it loses stability before that through a sub-critical Hopf bifurcation. However, the distance between the Hopf bifurcation and the saddle-node bifurcation, is so small, that we have chosen to omit it in our sketch. We again refer to Alkhayoun *et al.* for a more extensive bifurcation analysis.

To simulate the influx of fresh water we apply a time dependent, piece-wise linear hos-

ing function, $H(t) = H_{pwl}(t - t_0)$ (see Figure 2), to equations (7)-(10). Here

$$H_{pwl}(t) = \begin{cases} H_0 & t < 0, \\ \alpha(t) & t \in [0, T_{rise}], \\ H_{pert} & t - T_{rise} \in [0, T_{pert}], \\ \beta(t) & t - T_{rise} - T_{pert} \in [0, T_{fall}], \\ H_0 & t \geq T_{rise} + T_{pert} + T_{fall}, \end{cases} \quad (11)$$

where $\alpha(t)$ and $\beta(t)$ are linear functions ensuring continuity of $H(t)$. If we define the rise and fall rates, as

$$r_{rise} = \frac{|H_{pert} - H_0|}{T_{rise}} \quad \text{and} \quad r_{fall} = \frac{|H_{pert} - H_0|}{T_{fall}} \quad (12)$$

then

$$\alpha(t) = r_{rise}t \quad \text{and} \quad \beta(t) = r_{fall}(t - T_{rise} - T_{pert}) \quad (13)$$

As demonstrated by Alkhayoun *et al.* whether the system undergoes a transition from one stable state to the other, is dependent not only on the value of H_{pert} , but on the rise and fall rates, r_{rise} and r_{fall} , as well as the perturbation time T_{pert} . In particular, they demonstrate that even when H_{pert} is above the bifurcation value that destabilizes the upper equilibrium branch, the system may still return to this equilibrium, provided T_{fall} is short enough; a process which they termed *avoided B-tipping*. In addition, they showed that if T_{pert} is too short, the system will not tip, but return to the initial equilibrium branch.

In what follows, we will apply the Υ indicator as described in the previous section to time series data generated by the 3-box model. We will separately study time series undergoing rate-, noise- and bifurcation-induced tipping, while attempting to assess the indicator's ability to gauge the stability of the time series as it approaches the tipping point. Before proceeding, we should clarify one point regarding noise-induced tipping, and what is meant by an early warning indicator in this context. Noise-induced tipping is inherently unpredictable, and hence one might conclude that any attempt at predicting such transitions is doomed to fail. However, although one cannot expect to develop an *early* warning indicator for these types of transitions, one should at the very least be able to tell, from time series data, once such a transition has occurred, i.e., when the unstable equilibrium branch has been crossed and the system is approaching a different equilibrium. The objective should

then be to develop an indicator that is able to identify this induced instability as soon as possible after the transition.

Finally, we note that, while it is possible to extend ARMA fitting to multivalued time series data, we have chosen to not go down that route, and instead only apply the indicator to a single time series for the salinity values from the North Atlantic basin, S_N . The reason for choosing S_N over S_T is that within the 3-box model, the equilibrium branches of S_N are that much further apart, making the transitions easier to see. Such a simplification might at first glance seem rather contrived, however we argue that, as the goal of any indicator is to be used on real-world time series data in which the connection to other time series is largely unknown, it is reasonable to only concentrate on one time series, despite the underlying system being multidimensional.

A. Bifurcation-induced Tipping

To induce B-tipping in the 3-box model, we gradually change $H(t)$ according to equation (11), with $H_0 = 0$, $H_{pert} = 0.5$, $T_{rise} = 1000$. We let T_{pert} go to infinity, such that $H(t)$ never returns to its initial value. As $H(t)$ changes, S_N follows the upper equilibrium branch as sketched in Figure 3, until it reaches the hopf-bifurcation (around $H = 0.4$), at which point the upper equilibrium branch becomes unstable, and S_N abruptly falls towards the lower equilibrium branch. We choose a window length of 350 points corresponding to about 70 time units.

Figure 4 shows the time series of S_N color coded according to the value of Υ , with brighter colors corresponding to higher values of Υ and hence a greater degree of instability. Figure 5 shows Υ as a function of time, with clear peaks corresponding to brightly colored points in Figure 4.

It should be noted that low amplitude white noise is also applied to facilitate ARIMA model fitting. The noise intensity is kept small enough to avoid noise-induced tipping. Figures 4 and 5 clearly indicate that there are several points on the time series as it approaches the transition, which are deemed to have a high degree of instability. However, this is slightly deceptive as when we look at the values for ΔBIC , Figure 6, it becomes clear that the large values of Υ correspond to negative ΔBIC values. We recall that this

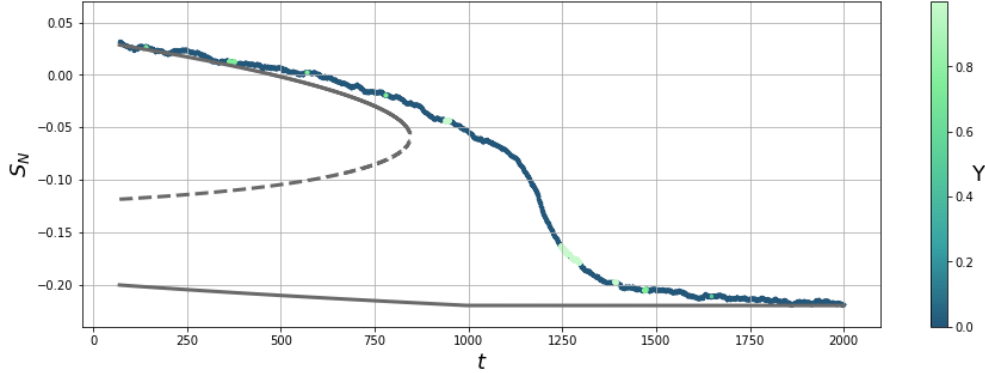


FIG. 4: Bifurcation-induced tipping, color coded according to the value of Υ with window length, $\tau = 350$. The gray lines denote the equilibrium branches, with the dashed line corresponding to the unstable branch. We clearly see several brightly colored points corresponding to a high values of Υ , which should be indicative of a high degree of instability and an approaching tipping point.

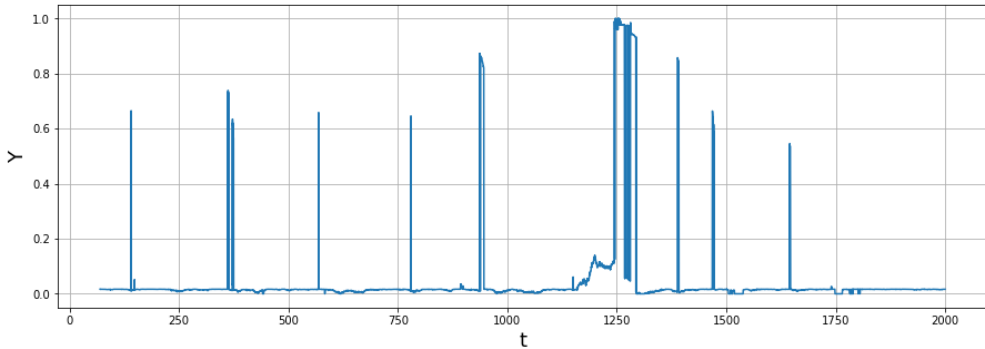


FIG. 5: Plot of Υ as a function of time for a time series of S_N undergoing B-tipping.

happens when the AR(1) process is excluded as the best model fit due to lack of stationarity (AR1 coefficient being too close to 1), despite having a smaller BIC value than the chosen fit. Figure 6 shows the time series of S_N color coded according to the value of ΔBIC with the negative values removed. We see that the value of ΔBIC is generally high (above the significance threshold), indicating a high degree of confidence in the chosen model fit, for the case of positive ΔBIC values. Also plotted is ΔBIC as a function of time, *including* the negative values. It is clear that the negative values dominate in absolute terms and are largely responsible for the peaks of Υ in Figure 5. This is unfortunate, as it makes the interpretation of the result unclear.

Hence, we need to look at the q and p values, as well as the persistence, to a make a proper

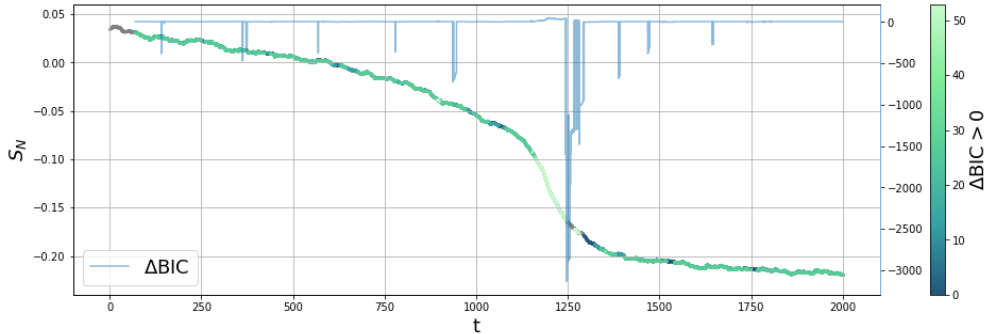
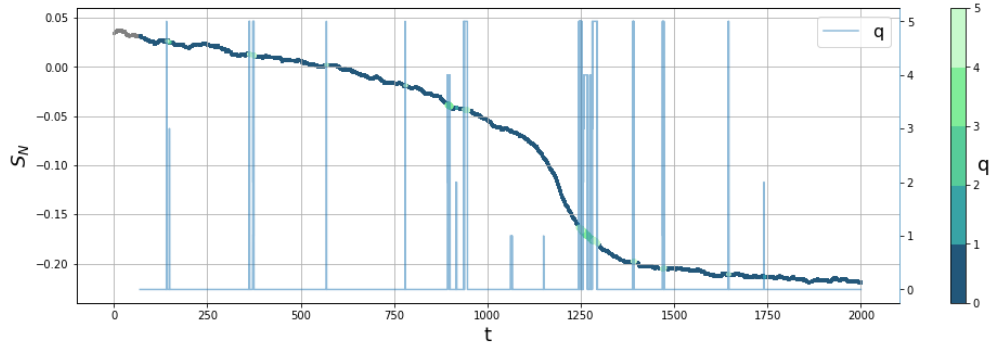


FIG. 6: Bifurcation-induced tipping of $S_N(t)$, color coded according to the value of $\Delta\text{BIC} = \text{BIC}(1, 0) - \text{BIC}(p, q)$ in which we have removed the negative values. This is to remove the points where, based solely on BIC value, the AR(1) process is a better fit than the selected ARMA(p,q) model. In these cases, the AR(1) model is rejected on other grounds, specifically because the absolute value of the AR1 coefficient is approaching 1. Included in the plot is the plot of ΔBIC including the negative values. As can be seen, the negative values dramatically dominate and are largely responsible for the spikes in Υ seen in Figure 5.

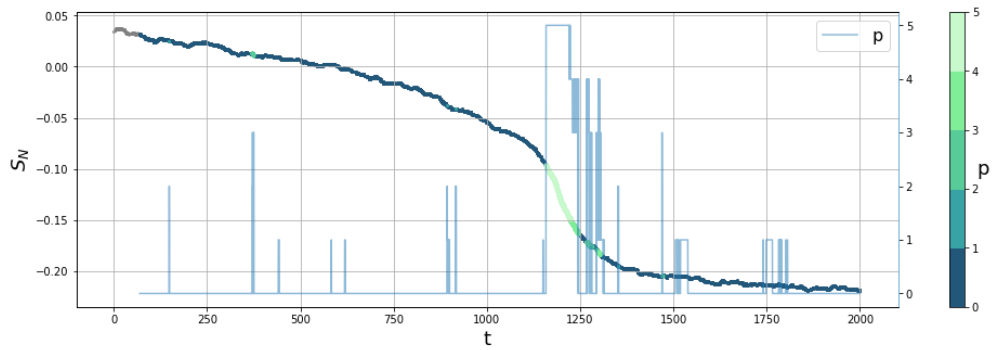
assessment of the stability properties of the time series. Figure 7 shows the time series of S_N color coded according to the values of q and p . When comparing with Figure 4, this seems to indicate that the high values of Υ appearing before the transition are primarily associated with an increase in the q -values. This is not unexpected, as it is primarily the change in the properties of the noise which is expected to give an indication of an approaching transition. Figure 8 shows the persistence plotted as a function of time t . We see a clear increase in the persistence directly preceding the tipping point around $t = 1000$.

We make a final comment regarding Figure 7 and its relation to our choice of AR(1) as the base model. In Faranda *et al.*⁹ this choice was guided by the fact that for the time series under consideration the order, i.e. $p + q$, of the intervals was clustered around 1, and as the authors explicitly excluded pure moving-average processes, they concluded that AR(1) was the appropriate base model. However, from Figure 7 we see that for the series currently under consideration, the order is clustered around 0, which corresponds to white noise possibly with a drift. Hence, there would be room to argue that the base model should be a white noise process and not the AR(1) process. However, we will refrain from making this change as we explicitly want to compare the fitted model with a Langevin process, which

The Υ indicator for Early Warning



(a)



(b)

FIG. 7: Bifurcation induced tipping of $S_N(t)$, color coded according to the value of (a) q and (b) p . The value for q and p are also plotted as functions of time in (a) and (b), respectively.

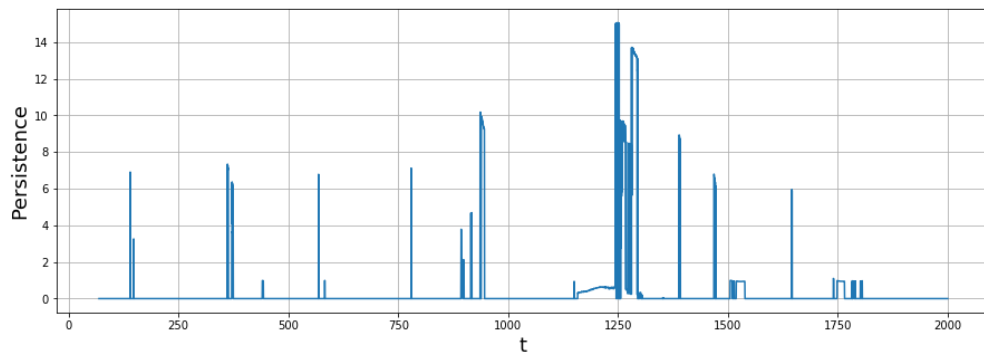


FIG. 8: Plot of the persistence as a function of time for a time series of S_N undergoing B-tipping.

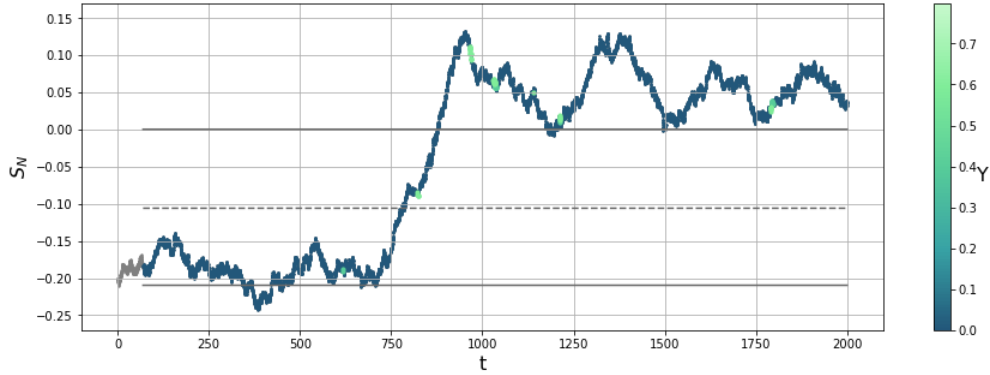


FIG. 9: Noise-induced tipping, color coded according to the value of Υ . The gray lines denote the equilibria, with the dashed line denoting the unstable equilibrium branch. Transition from the lower to the upper equilibrium branch for $H = -0.25$, $\tau = 352$.

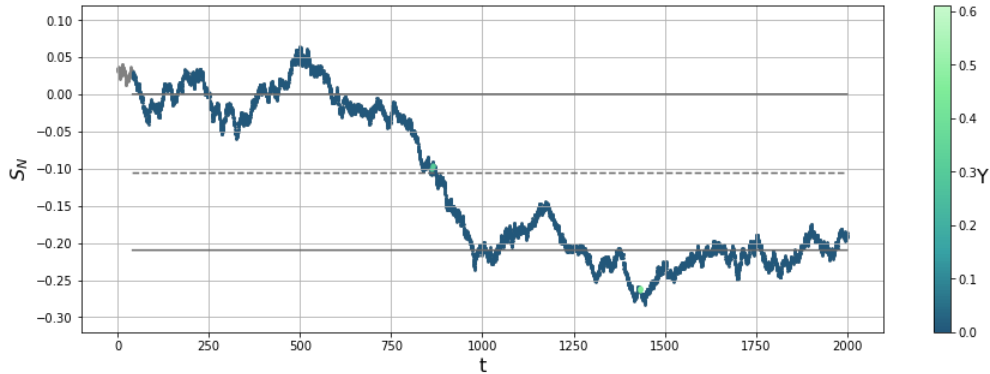


FIG. 10: Noise-induced tipping, color coded according to the value of Υ . The gray lines denote the equilibria, with the dashed line denoting the unstable equilibrium branch. Transition from the upper to the lower equilibrium branch for $H = 0.24$, $\tau = 208$.

when discretized is just an AR(1) process (see Nevo *et al.*¹⁰ for a detailed explanation of the argument).

B. Noise-induced Tipping

To induce N-tipping, we fix the hosing parameter H and apply additive noise to all the equations equally. We look at transitions from the upper branch to the lower branch and *vice versa*. In either case, it is convenient to choose a value for H that is close to the bifurcation point, as the probability of transitioning is much higher in these regions, and

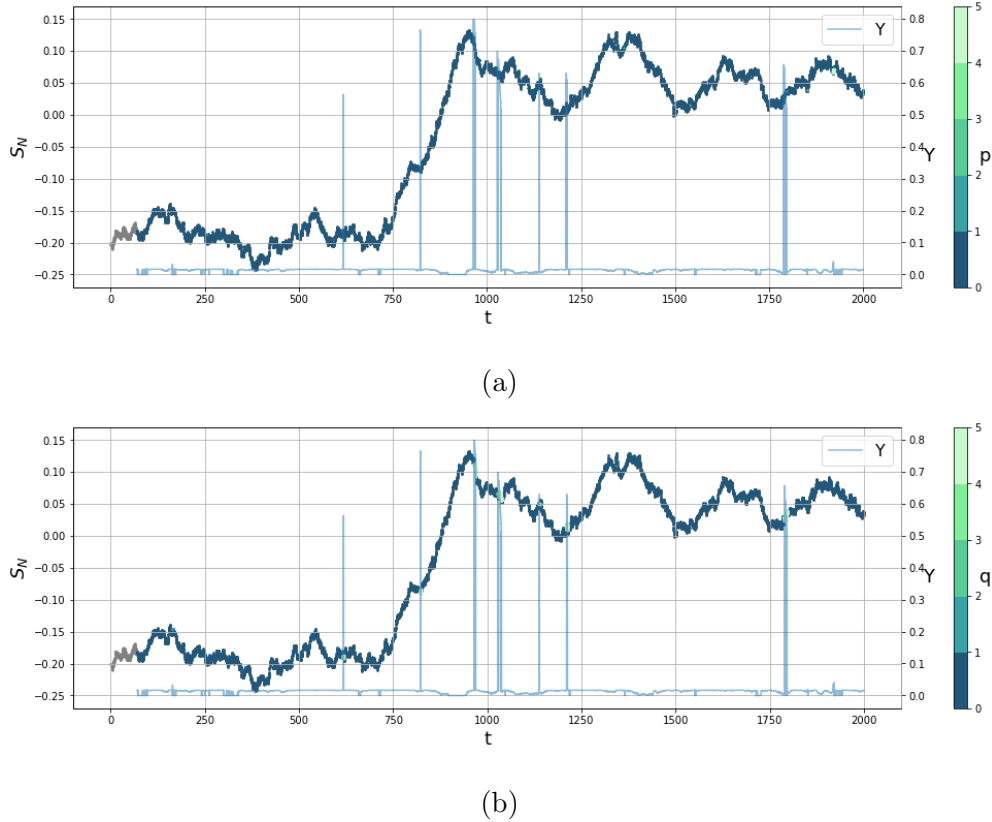


FIG. 11: Noise-induced tipping of $S_N(t)$ for $H = -0.25$, $\tau = 352$, color coded according to the value of (a) p and (b) q . Also plotted is Υ as a function of time.

hence one does not need high amplitude noise to induce transitions between the branches. Figures 9 and 10 show two time series undergoing noise induced tipping, one going from the lower to the upper branch, while the other going the other way around. In the first case $H = -0.25$, while in the second $H = 0.24$. The amplitude of the additive white noise is the same in both cases. For the window length τ , we have chosen a length of 352 and 208 points, corresponding to about 70 and 41 time units, respectively. The window length is chosen so that it is at most half as long as the transition time, which is taken to be the time for the system to arrive at the other equilibrium once it has crossed the unstable branch. Of course, when dealing with simulation data such as this, we have the advantage of knowing where the stable and unstable branches are, which is an advantage that anyone dealing with real-world data does not have. In principle one could use the clustering methods proposed by Kaiser *et al.*¹¹ to approximate the window length, although this method also requires that one knows how many clusters, i.e., equilibrium states, one should look for. The clustering

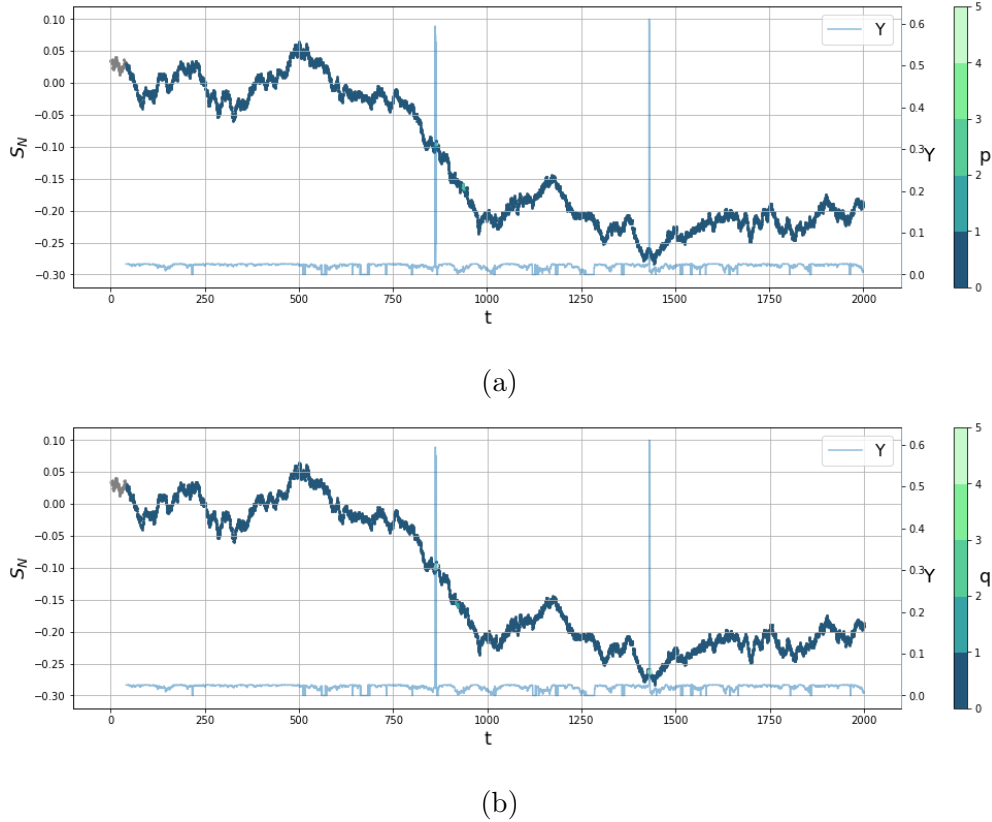


FIG. 12: Noise-induced tipping of $S_N(t)$ for $H = 0.24$, $\tau = 208$, color coded according to the value of (a) p and (b) q . Also plotted is Υ as a function of time.

method works particularly well for noise induced transitions, as one can repeatedly induce transitions back and forth, to gain an ensemble of transitions, yielding a higher degree of accuracy.

In previous works, the choice of τ has largely been guided by a desire to ensure the stationarity of the time series intervals. However, as we are not requiring the individual time series segments to be stationary *a priori*, we are permitted to use much longer time series intervals. In the world of ARIMA fitting a time series of length above 200 points would generally be considered a very long series, however, we should keep in mind that the sampling frequency of our simulated data is quite high; in fact, there are 5 points per time unit, yielding a total of 10000 points. Thus, as already given explicitly above, an interval consisting of 200 points corresponds to around 40 years, which is not an unreasonably long time interval for the dynamics of the AMOC. When fitting an ARIMA model to a time series, one wishes to avoid too long time series to avoid including events from the past that no longer have

any relevance for the future. This, and not the inherent inaccuracy of the fit itself, is the primary reason for limiting the length of a time series.

Returning to Figures 9 and 10, we note that there are a few brightly colored points indicating a high degree of instability. There are for example, in both cases, several points in the middle of the gap between the two stable branches, indicated by solid gray lines in the figure. This is consistent with the results of Kaiser *et al.* In addition, for the transition from the lower to the upper branch, Figure 9, there are several brightly colored points just after the system has reached the upper equilibrium branch. Although it is not so clear in the figure due to the presence of noise, any time S_N returns to the upper equilibrium branch it initially overshoots and then oscillates around the equilibrium value with continuously decreasing amplitude (see Figure 14 for a clearer example of this behavior). This is probably due to the presence of an unstable limit cycle, and the aforementioned sub-critical hopf bifurcation. Hence, we see it as an encouraging sign that the indicator seems to be able to identify these points as well. However, again, when looking at the values for ΔBIC we notice that high values of Υ are associated with negative values for ΔBIC , just as for B-tipping in the previous subsection.

Thus, we need to look at the p and q values to get a notion of the actual stability properties of the time series. Looking at the p and q values in Figures 11 and 12, it is clear that high values of Υ correspond to high values of q , while the connection between p and Υ remains uncertain. Furthermore, we note that, although not explicitly shown, the high q values appearing around the transition correspond to high values of persistence.

C. Rate-induced Tipping

To induce R-tipping we fix H_{pert} below the bifurcation value, ensuring that both equilibria still exist and are stable, and vary T_{fall} . We set $T_{rise} = 100$ and $T_{pert} = 400$, while $H_{pert} = 0.37$. Then we observe that for $T_{fall} = 280$ the system returns to the upper equilibrium branch, while for $T_{fall} = 320$, the system transitions to the lower branch. The transition happens even though the bifurcation boundary has not been crossed. Again, we note that some additive white noise has been applied to allow for ARIMA fitting.

Figure 13 shows a time series undergoing rate-induced tipping, with the color coding cor-

The Υ indicator for Early Warning

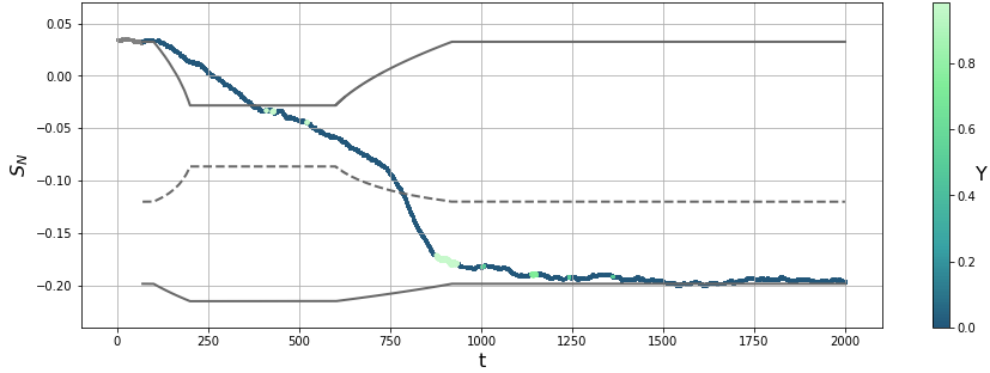


FIG. 13: Rate-induced tipping of S_N , color coded according to the value of Υ . The moving equilibria are plotted in gray, with the dashed line denoting the unstable branch. Compare this figure to Figure 17a, which shows the same time series, but color coded according to the value of q .

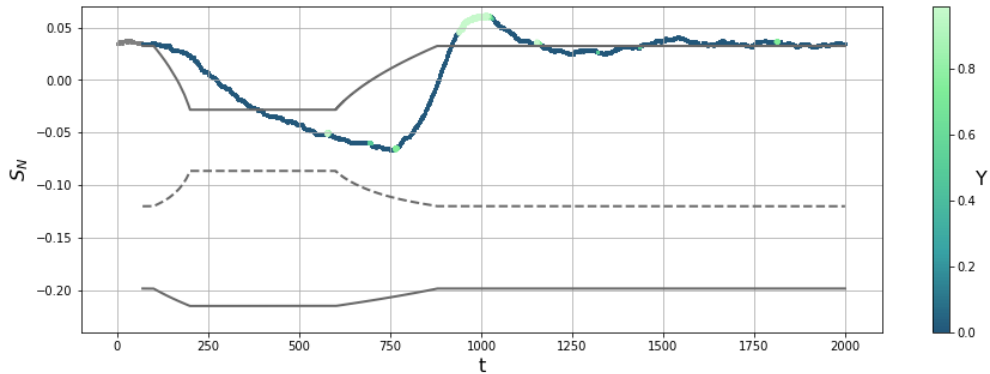


FIG. 14: S_N as a function of time, color coded according to the value of Υ for $T_{fall} = 280$. With these parameter values, the system does not tip, but returns to the upper equilibrium branch after some time. Note that the system initially overshoots the stable branch upon return. This is probably due to the presence of the unstable limit cycle. The equilibrium branches are plotted in gray, with the dashed line denoting the unstable branch.

responding to the values of Υ . Again, we have chosen $\tau = 350$ points, corresponding to 70 time units. We see several brightly colored points, indicating a high degree of instability, before the system transitions. These points occur initially as the system approaches the unstable branch. These points do not appear for the time series that does not tip, Figure 14, and could therefore be an indication of an approaching tipping point. Unfortunately, the ΔBIC values, Figures 15 and 16, are again negative for these specific points. Figure 15 and

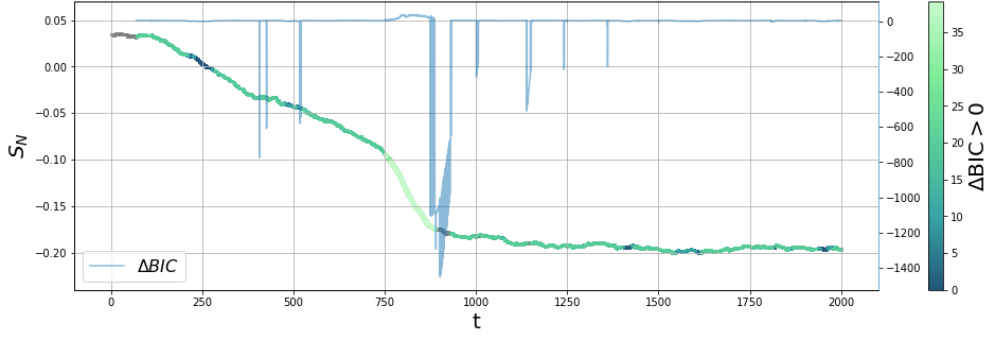


FIG. 15: S_N as a function of time, color coded according to the value of ΔBIC , where the negative values have been removed. Included is also the plot of ΔBIC as a function of time, *including* the negative values.

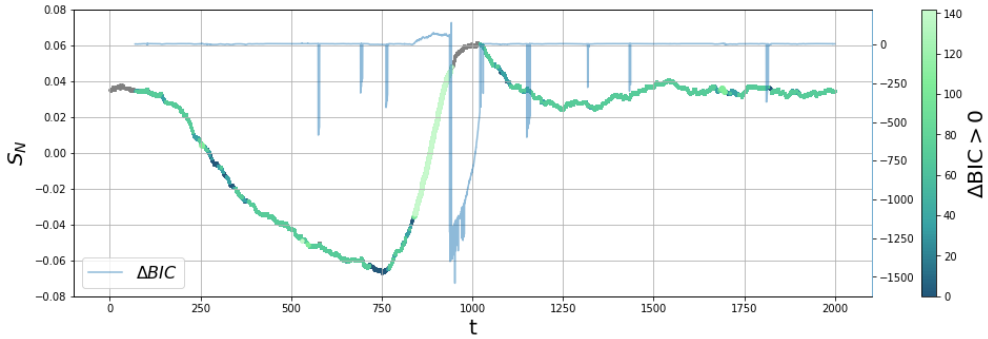
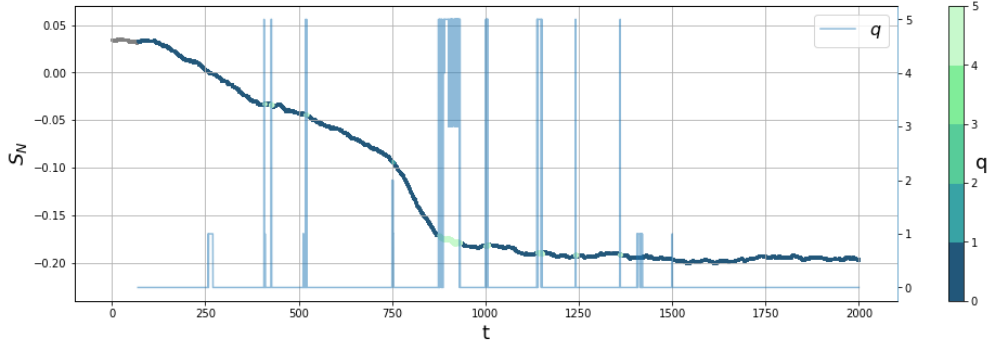


FIG. 16: S_N as a function of time, color coded according to the value of ΔBIC , where the negative values have been removed. Included is also the plot of ΔBIC as a function of time, *including* the negative values.

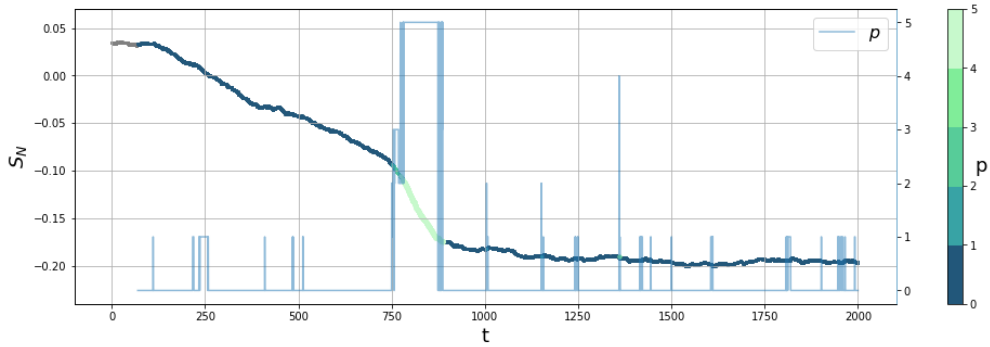
16 show the time series of S_N color coded according to the values of ΔBIC where we have excluded the negative values, as well as a plot of ΔBIC as a function of time *including* the negative values. It is clear from this plot that the negative values dominate and are largely responsible for the peaks in Υ found in Figures 13 and 14.

Thus, once more, we need to turn to other indicators to make a proper assessment of the stability properties of the time series. Looking at Figure 17, it becomes clear that the high values of Υ found in Figure 13 correspond to high values of q , while a comparison with Figure 19, gives the same indication for the persistence. In other words, high values of Υ primarily correspond to high values of persistence and q .

Looking at Figure 14, we can also see how the indicator correctly identifies the unstable limit cycle, which we have argued causes the overshoot when returning to the upper equilibrium



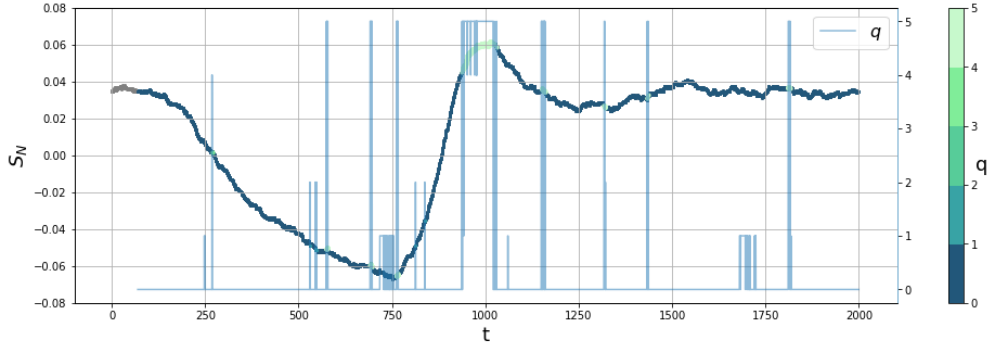
(a)



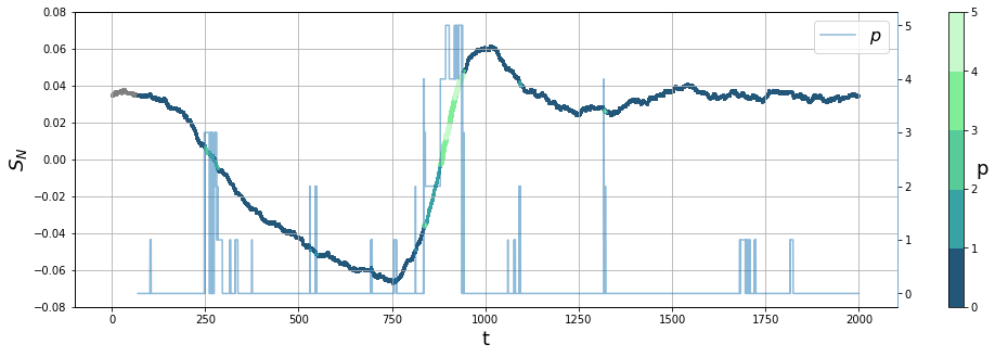
(b)

FIG. 17: Rate-induced tipping of $S_N(t)$, color coded according to the value of (a) q and (b) p . The value for q and p are also plotted as functions of time in (a) and (b), respectively.

branch. Figure 18 shows the same time series as in Figure 14, color coded according to the values of q and p . While high values of q seem to be associated with increased instability, the high values of p primarily occur as the system returns to the equilibrium. We would therefore suggest that high values of the autoregressive order, p , should be interpreted as an indication that the system is following a moving equilibrium branch. Thus, although the ΔBIC values are negative, we can still assess the change in the memory lag from the increase in the p and q values. Comparing Figures 19 and 17a it becomes clear that the points with high q value around $t = 1000$, correspond to particularly high values of persistence, even when compared to other points of similar order.



(a)



(b)

FIG. 18: S_N as a function of time, color coded according to the value of (a) q and (b) p , for $T_{fall} = 280$. For these parameter values, the system does not tip, but returns to the initial equilibrium after some time t . For clarity, p and q are also plotted as functions of time in (a) and (b), respectively. It is instructive to compare these plots to Figure 14.

IV. APPLICATION TO SIMULATION DATA FROM CESM2

So far, we have only applied the indicator to data from a very simplified model. The actual ocean has many more degrees of freedom and the response could be quite different. To examine this, we apply the measures to data from the earth systems model CESM2. We consider two scenarios: one in which the atmospheric CO_2 concentration is abruptly doubled and another in which it is abruptly quadrupled. Both simulations are initialized using a pre-industrial control run (*piControl*) and then run for 500 years. The data was saved at monthly intervals and the seasonal cycle was removed prior to the analysis. Note that the abrupt change in CO_2 represents an extreme forcing, and contrasts with the ramped-up hosing employed with the idealized model. However, the oceanic response is not instantaneous, but

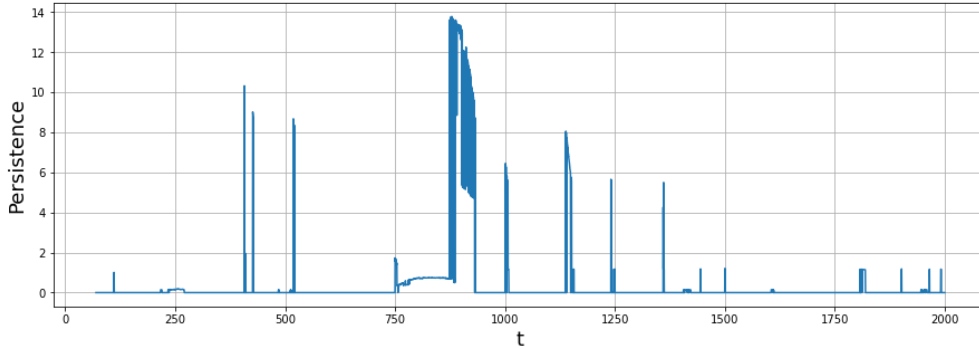


FIG. 19: Persistence of a time series undergoing rate-induced tipping, plotted as a function of time. The underlying series is the time series shown in Figure 13. We see several high persistence values, corresponding with a high value for the order, $q + p$ (compare with Figure 17), appearing before the potential tipping point around $t = 500$.

requires 2-3 decades for freshwater to circulate in the model's sub-polar gyre²⁸. We consider this more hereafter.

A. Abrupt $4 \times \text{CO}_2$

The time series of the monthly density difference, $\delta\rho$, and AMOC strength, ψ_{AMOC} , in the case of abrupt $4 \times \text{CO}_2$ is shown in Figure 20. The density difference, a measure dynamically linked to the AMOC strength (Madan *et al.*²⁸), is calculated from the difference in surface densities averaged in boxes to the north and south of the North Atlantic Current. The surface density term is calculated using the thermodynamic equation of state of seawater as per UNESCO 1983 Report²⁹. The AMOC strength is calculated as the monthly maxima of meridional overturning stream function between $20^\circ N$ - $60^\circ N$ and below 450 m depth. Shortly after the quadrupling of the CO_2 concentration, there is an abrupt transition followed by a dramatic increase in the variance. We will only apply the indicator to the density difference time series, although one could in principle apply the same analysis to the AMOC strength data.

We choose a window length of 250 data points, corresponding to exactly 20 years of monthly data. Figure 21 shows the density difference, $\delta\rho$, color coded according to the values of Υ . We are only displaying the part of the time series close to the transition, as this is the part which interests us the most. The increase in Υ during the early part of the transition is

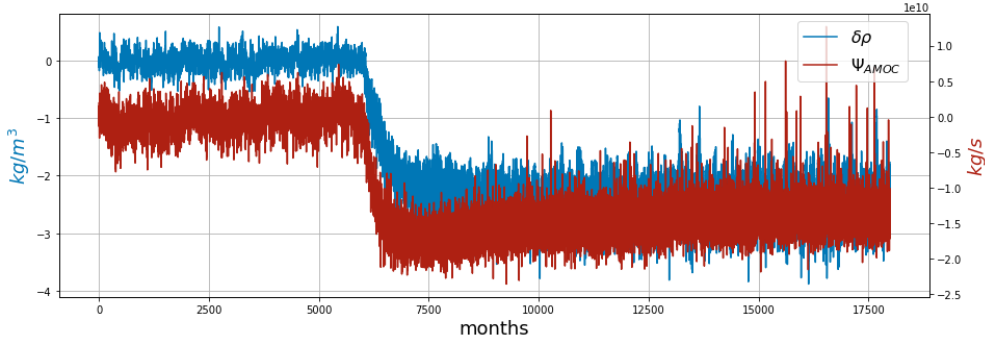


FIG. 20: CESM2 model with abrupt $4 \times \text{CO}_2$, where the monthly density difference (blue) is plotted together with the maximum AMOC flow strength (red).

apparent. Note in particular the three sharp peaks shortly after time $t=6000$. It should be emphasized that in this case, the peaks are not indicative of negative ΔBIC values, as we saw in the case of the 3-box model. In fact, negative ΔBIC values do not occur at all for this time series. Figure 22 again shows the time series, this time color coded according to the values of q and p . The time series of q and p are also plotted for further clarification. From this plot, it comes clear that the most common fit prior to the transition is the AR(1) process, which aligns with the observations of Faranda *et al.*⁹. After the transition, the value of p is generally an order higher, presumably related to the dramatic increase in the variance. The three sharp peaks in the plot of Υ appearing around time $t = 6300$ correspond to high values of q . The gradual increase in Υ preceding these peaks is presumably due to the increase in the persistence (not shown). Following the transition, the value for Υ remains high, probably a result of the increase in the p value. However, the values of Υ do not go above 0.4 which is considerably smaller than the values found for the 3-box model. Presumably, this is correlated with the lack of negative ΔBIC values, since, as we recall, the peaks in the 3-box model corresponded to cases with negative ΔBIC values resulting from the AR1 coefficient approaching 1.

For completeness, we have included a comparison between Υ and two other statistical early warning indicators, namely autocorrelation and variance. This is shown in Figure 23. In all cases, the window length is 250 points, corresponding to approximately 20 years. All three indicators show a clear increase shortly after time $t = 6000$. For a proper explanation of how we have computed the autocorrelation and variance, we refer the reader to the next section of the paper, where the indicators are formally compared.

The Υ indicator for Early Warning

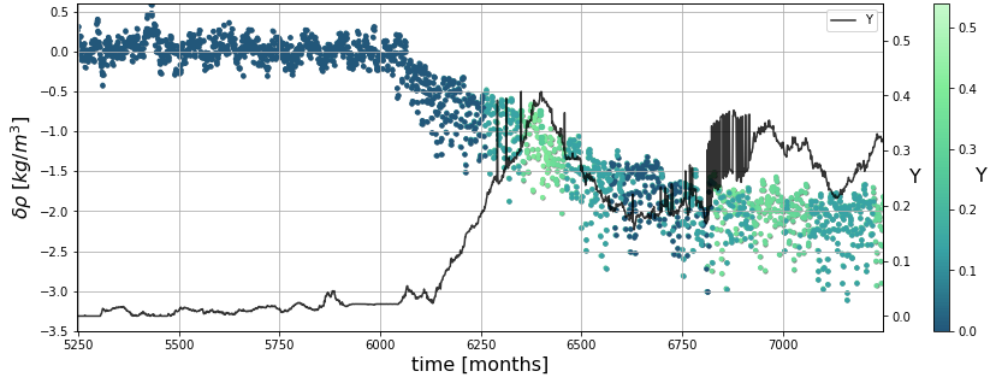
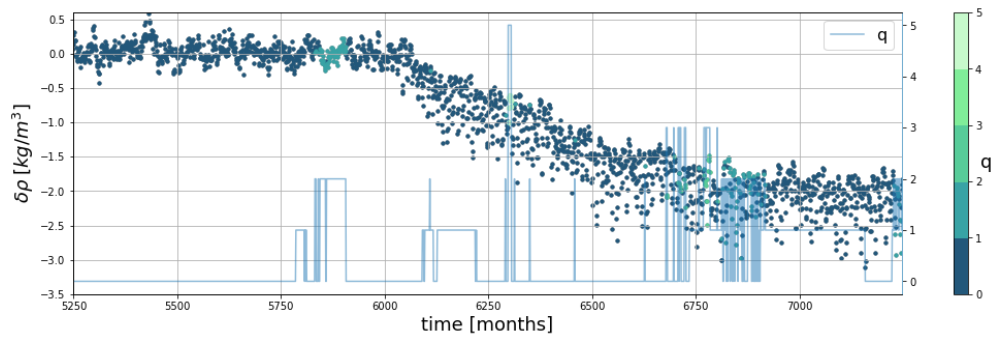
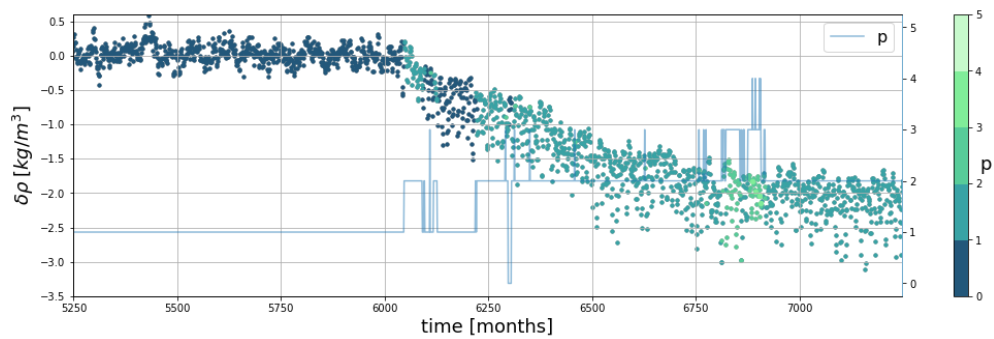


FIG. 21: Time series of monthly density changes for abrupt $4 \times \text{CO}_2$, color coded according to the value of Υ . The window length is 250 points, corresponding to exactly 20 years.



(a)



(b)

FIG. 22: Time series of monthly density changes for abrupt $4 \times \text{CO}_2$, color coded according to the value of (a) q and (b) p . The value for q and p are also plotted as functions of time in (a) and (b), respectively.

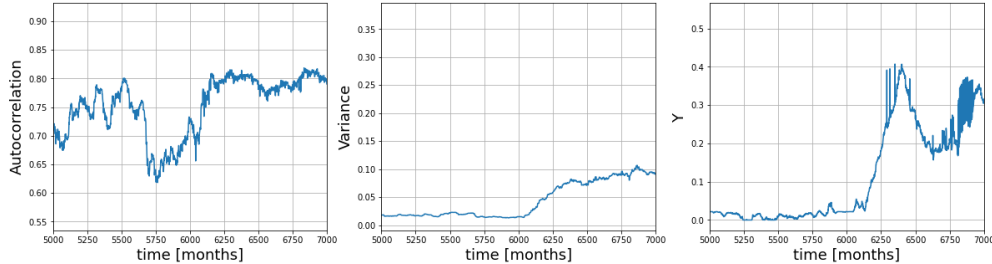


FIG. 23: Autocorrelation, variance and Υ plotted as functions of time for the case of abrupt $4 \times \text{CO}_2$.

B. Abrupt $2 \times \text{CO}_2$

The time series of the monthly density difference, $\delta\rho$, and AMOC strength, ψ_{AMOC} , in the case of abrupt $2 \times \text{CO}_2$ is shown in Figure 24. Again, we only apply the indicator to the density difference data, and choose the same window length as in the case of abrupt $4 \times \text{CO}_2$. Figure 25 shows an excerpt of the density difference time series close to the transition, as well as a plot of the Υ values. The point at which the CO_2 concentration is abruptly increased is denoted with a dashed line. The first thing to note is how small the Υ values are compared to what we have seen previously; on the order of 10^{-2} . It should, however, be noted that the ΔBIC values are well above the significance threshold. Figure 26 shows the density difference time series color coded according to the value of q and p . From this, we again see that prior to the increase in CO_2 , the most common fit is the AR(1) process, while after the transition the p values show a clear increase. The q value, on the other hand, does not go above 2, indicating a very low degree of memory in the noise term. Since we have by now clearly demonstrated a correlation with the value of Υ and the value of q , this should provide an explanation as to why we see such low values of Υ . From this analysis, one would conclude that the system does not appear to be approaching a tipping point. Once more we have, as shown in Figure 27, included a comparison with other early warning indicators. The autocorrelation and variance show a dramatic increase around time $t=6000$, which corresponds to the appearance of the cluster of sharp peaks in the time series plot for Υ .

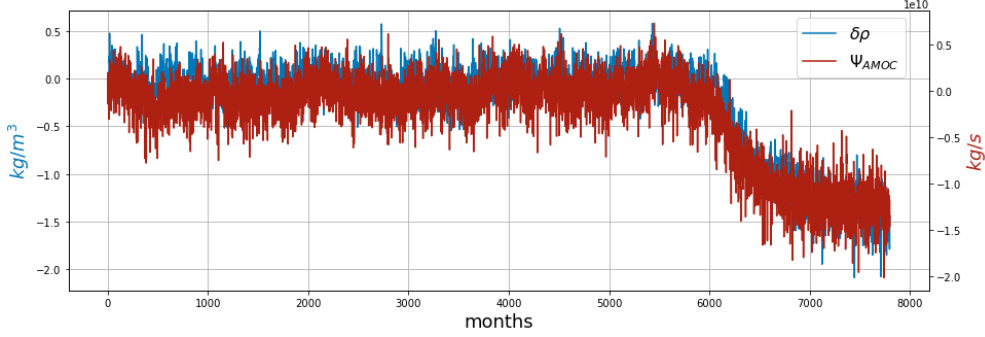


FIG. 24: CESM2 model with abrupt $2 \times \text{CO}_2$, where the monthly density difference (blue) is plotted together with the maximum AMOC flow strength (red).

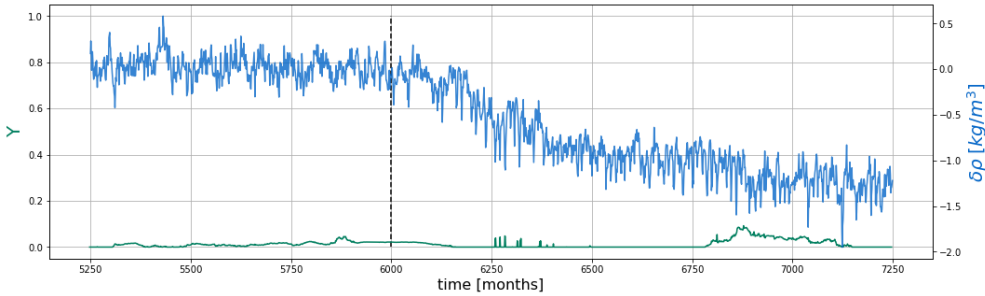
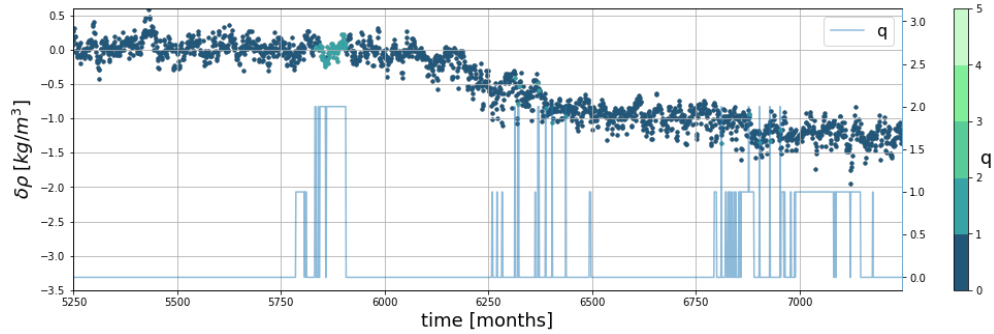


FIG. 25: Monthly density changes, $\delta\rho$, for abrupt $2 \times \text{CO}_2$ (blue) and the value of Υ (green) plotted as functions of time. The dashed line indicates the point when the CO_2 concentration abruptly changes.

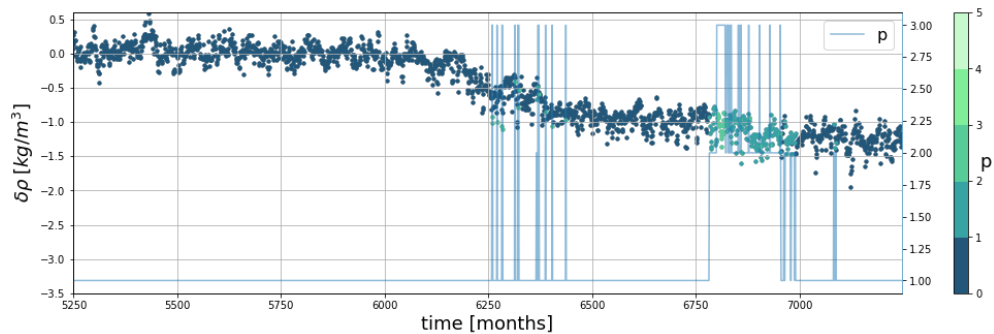
V. COMPARISON WITH OTHER EARLY WARNING INDICATORS

As briefly alluded to in the introduction, it is well established that bifurcation-induced tipping is generally preceded by an increase in lag 1 autocorrelation and variance (Lenton *et al.*³⁰, Dakos *et al.*³¹, Boers²³). The intuition behind this is that as the system approaches a bifurcation point, the potential well flattens out, reducing the speed at which the system recovers from a perturbation, so called "critical slowing down", which should manifest as an increase in the variance and autocorrelation of the time series. However, the variance and autocorrelation might also increase for other reasons, in particular if the properties of the noise changes. What happens to the autocorrelation and variance when the system approaches a rate-induced tipping point is thus far unclear, although it is conceivable that the "critical slowing down" hypothesis still holds for this type of tipping, see Ritchie and Sieber⁸. Obviously, it does not hold true for time series undergoing noise induced tipping,

The Υ indicator for Early Warning



(a)



(b)

FIG. 26: Time series of monthly density changes for abrupt $2 \times \text{CO}_2$, color coded according to the value of (a) q and (b) p . The value for q and p are also plotted as functions of time in (a) and (b), respectively.

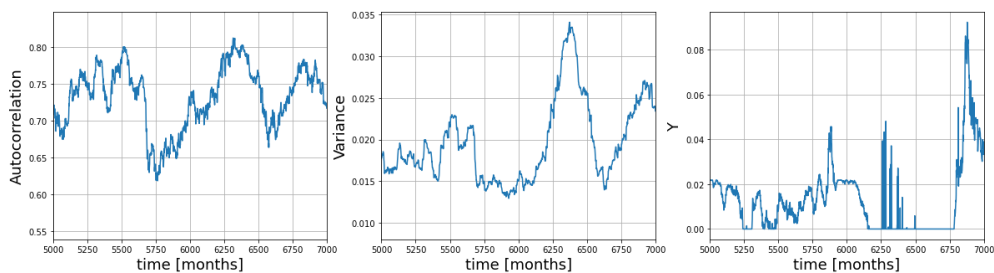


FIG. 27: Autocorrelation, variance and Υ plotted as functions of time for the case of abrupt $2 \times \text{CO}_2$

as there is no change in the potential well. However, the autocorrelation and variance of the time series will dramatically change as the system crosses the unstable equilibrium branch and enters a different potential well.

In what follows, we will compare these classical indicators to the Υ indicator for rate-induced

and bifurcation-induced tipping in the AMOC 3-box model; we have already included a comparison for the CESM2 data in the previous section. In these cases, it is instructive to just look at the part of the time series prior to the transition, as in general one wishes to be able to predict the transition *before* it happens. For the time series undergoing bifurcation-induced tipping (Figure 4) we chose a segment consisting of the points between approximately $t = 200$ and $t=1100$. For the time series undergoing rate-induced tipping (Figure 13), we choose a segment consisting of the points between $t = 200$ and $t = 700$. This segment is in all probability too long, meaning that it also contains the transition itself, as opposed to only points prior to the transition. However, this is the inherent difficulty with rate induced tipping; there is currently no way to analytically determine *when* the transition happens, and one largely has to guess. Based on Figures 13 and 14, one could potentially conclude that the tipping point is found somewhere between $t = 400$ and $t = 600$, but this is pure guess work. For this reason we have included points up until $t = 700$.

Given a set of measurements Y_1, Y_2, \dots, Y_N the variance is defined as

$$\sigma^2 = \frac{1}{N} \sum_{i=1}^N (Y_i - \bar{Y})^2 \quad (14)$$

while the lag k autocorrelation is given by

$$r_k = \frac{1}{N\sigma^2} \sum_{i=1}^{N-k} (Y_i - \bar{Y}) (Y_{i+k} - \bar{Y}) \quad (15)$$

where \bar{Y} denotes the mean of the series Y_1, Y_2, \dots, Y_N . Although time does not enter explicitly in the formulas, it is assumed that the measurements are taken at regular intervals.

When computing the variance and autocorrelation it is essential that the signal is properly detrended; otherwise any trend will immediately obscure the relevant dynamics. As for the Υ indicator, one generally employs a rolling window approach, with an appropriately chosen window length τ . Lenton *et al.*³⁰ demonstrated that detrending can be done within each time window, as opposed to on the whole time series at once, without significantly changing the result. We have chosen this same approach, using linear detrending, as opposed to quadratic or higher order detrending methods, to remove the trend. The window length τ was set to 350 points, corresponding to 70 time units.

The Υ indicator for Early Warning

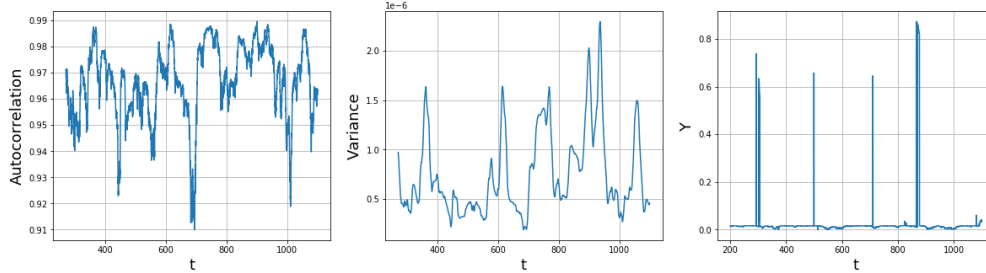


FIG. 28: Autocorrelation, Variance and Υ plotted as functions of time for a time series undergoing B-tipping. The increase in the variance as one approaches the tipping point is clear, while the increase in autocorrelation is less clear.

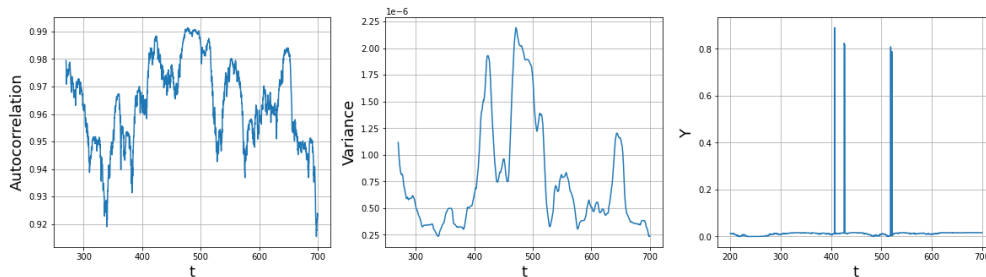


FIG. 29: Autocorrelation, Variance and Υ plotted as functions of time for a time series undergoing R-tipping. Assuming that the tipping point is around $t=450$, one can clearly see an increase in both autocorrelation and variance prior to the tipping point.

Figures 28 and 29 show the autocorrelation, variance and Υ plotted as functions of time. The peaks in Υ preceding the transition are clear, as is the increase in variance and autocorrelation, at least in the case of R-tipping, provided the tipping point is approximately at $t = 450$. For B-tipping, there appears to be a clear increase in the variance preceding the tipping point, provided the tipping point happens around $t = 850$ (see Figure 4 for comparison). The expected increase in autocorrelation is, however, less clear.

Compare this to Figures 23 and 27 which contain the same plots for the CESM2 data. In the latter case, the increase in variance and autocorrelation is obvious.

Comparing the autocorrelation plots for the 3-box model and the CESM2 data, we see that in the former case the autocorrelation is generally a lot higher. The high degree of autocorrelation could explain why the AR1 model is so readily rejected for the 3-box model time series data, resulting in the appearance of negative ΔBIC values.

As already noted, the upper equilibrium branch does not lose stability due to a saddle node

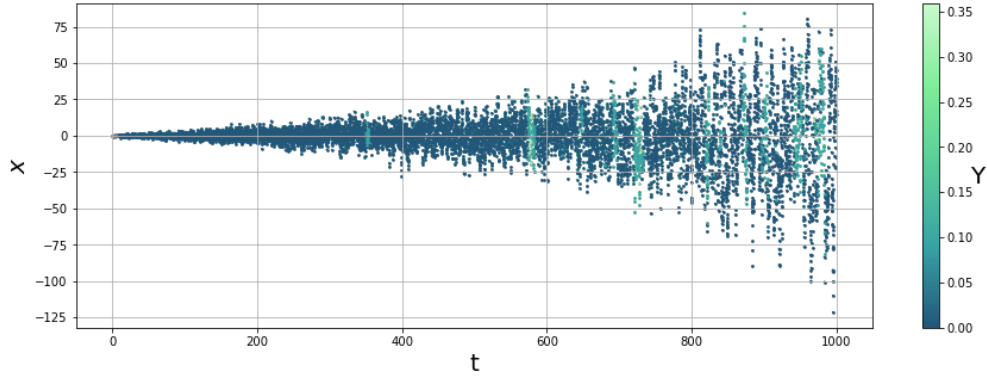


FIG. 30: Time series with colored noise but no tipping points, color coded according to the value of Υ .

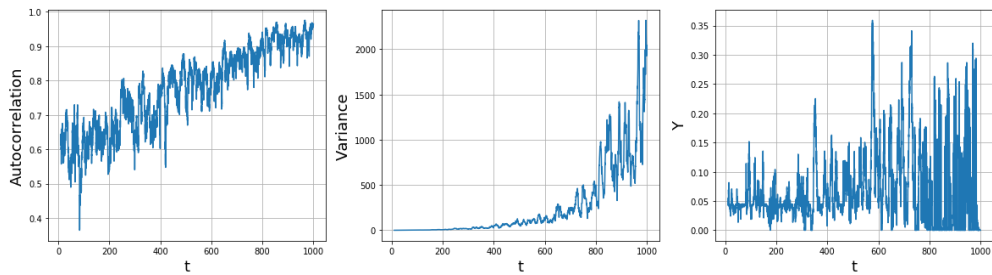


FIG. 31: Autocorrelation, Variance and Υ plotted as functions of time for a time series with colored noise but no tipping points. All three indicators show a dramatic increase, falsely suggesting an upcoming tipping point.

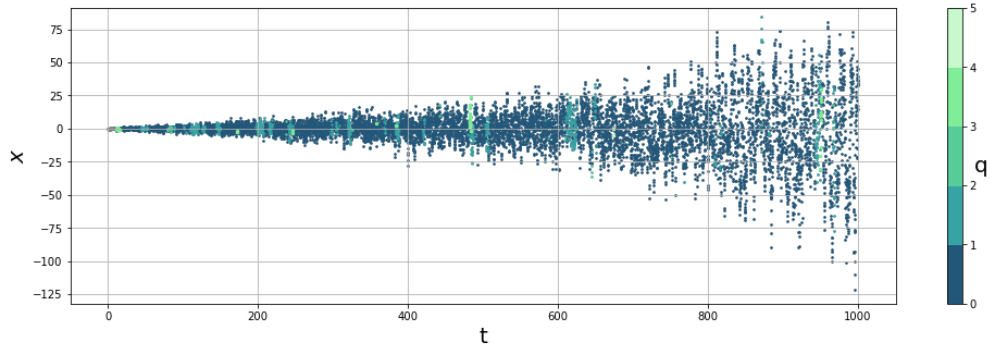
bifurcation, but rather loses stability due to a sub-critical Hopf bifurcation. It is possible that classical indicators are struggling to pick up on this. Furthermore, the noise amplitude is kept low to avoid noise-induced tipping, which might make it difficult for the indicators to pick up on changes in the dynamics.

As already mentioned, the autocorrelation and variance of a time series can increase for reasons that have nothing to do with an approaching tipping point. Hence, we wish to see how the Υ indicator responds to colored noise, whose variance and autocorrelation increases with time t . To this end, we construct an artificial time series of the form

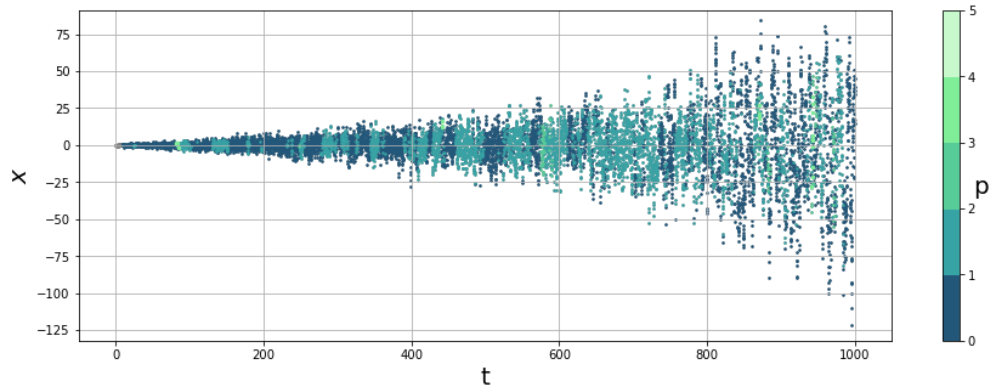
$$\frac{dx}{dt} = -5x + \xi(t) \quad (16)$$

where $\xi(t)$ is autocorrelated colored noise. $\xi(t)$ is in effect modelled as an AR(1) process whose AR1 coefficient increases linearly in time. In addition, the variance of this process

The Υ indicator for Early Warning



(a)



(b)

FIG. 32: Time series with colored noise and no tipping points, corresponding to equation (16), color coded according to the value of (a) q and (b) p .

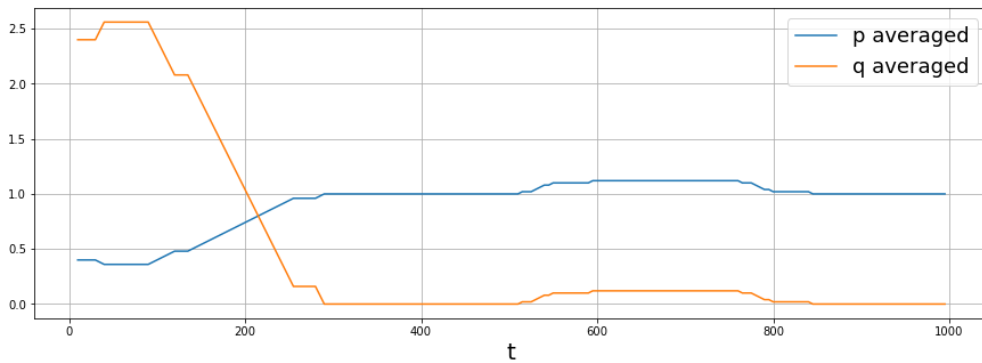


FIG. 33: The values of p and q for the colored noise time series, averaged with a window length of 50 points, corresponding to 25 time units.

also increases linearly in time. This is equivalent to the example presented in Boers²³. Applying the Υ indicator to this time series yields the result shown in Figure 30. Figure 31 shows a comparison between the autocorrelation, variance and value of Υ for the same time series. All three indicators show a dramatic increase, despite there being no approaching tipping point. However, looking at the plot of the time series when color coded according to the values of p and q , Figure 32, a curious pattern emerges: the increase in Υ is largely associated with increased p value. Looking at Figure 33 the trend becomes even clearer: here we have computed the rolling average of the p and q values with a window length of 50 points corresponding to 25 time units. We see that while the average value of q goes towards zero for large t , the average value of p settles around one. The general trend is independent of the choice of window length, provided the window length is between 30 and 300 points. This behavior is unlike what was observed for the 3-box model. The high values of Υ were associated with a high value of q . We thus argued that high values of q were associated with increased instability, while high values of p were more indicative of the system following a moving equilibrium. For the CESM2 data in the case of $4 \times \text{CO}_2$, we observed, see Figure 25, that after the transition the Υ values remained high, which we argued was due to the increased p value. As we can assume that the noise in this time series is autocorrelated, it is possible that it is the increased degree of autocorrelation in the noise, as opposed to a non-linear change in the dynamics, that the indicator is picking up on.

Thus, one would, through the distinction between q and p values, potentially have a way of distinguishing the effect of colored noise from real early warning signals. However, it is conceivable that the result for the artificial colored noise time series is a consequence of how we have constructed the colored noise, so further studies on this are warranted.

Finally, we note that the constructed colored noise time series is a very artificial example of colored noise, as the noise amplitude increases by a probably unrealistic amount, and when applied to any reasonable time series it would obscure the dynamics altogether. This is to say that although we can likely assume that the noise in real-world data is autocorrelated, it will be much more subtle, and not result in equally high values of Υ . In addition, although the increase in Υ is clear, it still only reaches a value of around 0.35, which is significantly lower than the values found in the 3-box model, although comparable to the values found for the CESM2 data.

TABLE I

| | Volume | Salinity | Flux |
|-------------------|---|---------------------|------------------------------|
| North Atlantic | $V_N = 0.3683 \times 10^7 \text{ m}^3$ | $S_N = 0.034912$ | $F_N = 0.486 \text{ Sv}$ |
| Tropical Atlantic | $V_T = 0.5418 \times 10^7 \text{ m}^3$ | $S_T = 0.035435$ | $F_T = -0.997 \text{ Sv}$ |
| Southern Ocean | $V_S = 0.6097 \times 10^7 \text{ m}^3$ | $S_S = 0.034427$ | $F_S = 1.265 \text{ Sv}$ |
| Indo-Pacific | $V_{IP} = 1.4860 \times 10^7 \text{ m}^3$ | $S_{IP} = 0.034668$ | $F_{IP} = -0.754 \text{ Sv}$ |
| Bottom Ocean | $V_B = 9.9250 \times 10^7 \text{ m}^3$ | $S_B = 0.034538$ | |

TABLE II

| name | default value | units | name | default value | units |
|----------|---------------|------------------------|-----------|--------------------|------------------------|
| α | 0.12 | kg/(m ³ °C) | K_N | 1.762 | Sv |
| β | 790.0 | kg/m ³ | K_S | 1.872 | Sv |
| S_0 | 0.035 | | λ | 1.62×10^7 | m ⁶ /(kg s) |
| T_S | 7.919 | °C | γ | 0.36 | |
| T_0 | 3.870 | °C | | | |

VI. DISCUSSION

In summary, we have applied the statistical indicator known as the Υ *indicator*, defined by equation (3), to time series data from a simplified model of the Atlantic overturning oscillation, the 3-box model, and from a full Earth-Systems Model, the CESM2. For the 3-box model, we looked at bifurcation-induced, noise-induced and rate-induced tipping separately, attempting to explore how the indicator reacts to different types of tipping in this very controlled setting. We have demonstrated that high values of the Υ indicator,

implying a high degree of instability, correspond primarily to high values of the order of the moving-average term, q , and increased persistence. It is not unexpected that an increase in the order should be correlated with an increase in the persistence. That the increase in dynamic instability, as measured by the Υ indicator, is primarily correlated with changes in the moving-average part of the series expansion, is not unexpected as the loss of stability should, in theory, manifest itself as a reduction in the system's ability to recover quickly from perturbations, and hence, the memory effect should primarily be found in the noise term. We argued that this could provide a way to distinguish real early warning signals from the effect of autocorrelated noise, as from our analysis the autocorrelated noise is characterized by high values of the autoregressive order, p .

By looking at the ΔBIC values directly, we were also able to determine that the values for Υ could in general be considered statistically significant, in the sense that the chosen ARMA(p,q) model is a significantly better fit than the AR(1) process that we chose as our base model. However, transitions in the 3-box model seemed to be largely characterized by a loss of stationarity of the AR1 process, yielding large negative ΔBIC values. While we have not been able to explain exactly why this happens for some time series, but not for others, we suggested the high degree of lag 1 autocorrelation of these time series as a possible explanation for the behavior.

When applied to the CESM2 data, the measure shows consistently lower values of Υ , and the indications of transition are less clear. This may be a consequence of having a far higher number of degrees of freedom in CESM2 than in the box models. Indeed, it is possible the model AMOC is tracking a continuously shifting steady state, rather than making a transition between two distinct states. This would be in line with other members of the CMIP6 ensemble exhibiting very different AMOC weakening from the same forcing²⁸. The difference could also be related to the CO2 forcing, which is applied abruptly. This could for instance induce an overshoot of a tipping threshold, obscuring the behavior³². However, the abruptness is likely not as severe as it seems as the CO2 forcing triggers a series of events, including sea ice melt and freshwater injection into the model's subpolar gyre, which occur over 2-3 decades²⁸. In any case, further study is required, perhaps with additional runs with more gradual CO2 changes.

The primary drawback of the Υ indicator is that it is computationally quite expensive, at least compared to the autocorrelation and variance, and that, due to its complexity, the results can be harder to interpret. We therefore suggest that the indicator should be applied with care, and preferably in combinations with other measures of instability, like the increase in the order, $p + q$, and the persistence. One should also take care to keep track of the ΔBIC values, as the potential for negative values can make the results hard to interpret. Although the current scaling with τ , see equation (3), seems to yield reasonable results, it is certainly possible that another scaling would be preferred. It is also possible that this is problem-dependent. This uncertainty regarding the correct scaling is certainly a drawback, but we argue that this problem can largely be circumvented by including an examination of the persistence and order values. However, it would still be advantageous to have an indicator whose values were to have a clear meaning in terms of the stability of the system, and it is not clear if the Υ indicator as it stands achieves this, partly due to the aforementioned issue with the choice of the correct scaling.

We conclude by noting that it is conceivable that one would wish to exclude white noise and pure moving-average, MA(1), processes when doing the fitting, as was done in the earlier studies by Faranda *et al.*⁹. We have, in the present study, chosen not to do this and instead used the thoroughly tested `auto.arima` function from the FORECAST R package. This choice is largely a matter of convenience, and we acknowledge the potential drawbacks.

ACKNOWLEDGMENTS

This research has been partly funded by the Deutsche Forschungsgemeinschaft (DFG) through grant CRC 1114 „Scaling Cascades in Complex Systems“, Project Number 235221301. Josph Henry LaCasce was supported in part by the Rough Ocean project, number 302743, from the Norwegian Research Council.

The computations for CESM2 data were performed on resources provided by Sigma2 - the National Infrastructure for High Performance Computing and Data Storage in Norway.

The authors thank Davide Faranda for stimulating discussions.

DATA AVAILABILITY STATEMENT

The data that support the findings of this study are available from the corresponding author upon reasonable request.

REFERENCES

- ¹P. Ashwin, S. Wieczorek, R. Vitolo, and P. Cox, “Tipping points in open systems: bifurcation, noise-induced and rate-dependent examples in the climate system,” *Phil. Trans. R. Soc. A* **370**, 1166–1184 (2012), doi:10.1098/rsta.2011.0306.
- ²M. Scheffer, E. H. Van Nes, M. Holmgren, and T. Hughes, “Pulse-driven loss of top-down control: the critical-rate hypothesis,” *Ecosystems* **11**, 226–237 (2008), doi:0.1007/s10021-007-9118-8.
- ³S. Wieczorek, P. Ashhwin, C. Luke, and P. M. Cox, “Excitability in ramped systems: The compost-bomb instability,” *Phil. Trans. R. Soc. A* **467**, 1243—126 (2011).
- ⁴P. E. O’Keeffe and S. Wieczorek, “Tipping phenomena and points of no return in ecosystems: Beyond classical bifurcations,” *SIAM Journal on Applied Dynamical Systems* **19**, 2371–2402 (2020).
- ⁵S. Wieczorek and C. Perryman, “Adapting to a changing environment: Non-obvious thresholds in multi-scale systems,” *Proc. R. Soc. A* **470**, 20140226 (2014).
- ⁶P. Ashwin, C. Perryman, and S. Wieczorek, “Parameter shifts for nonautonomous systems in low dimension: bifurcation- and rate-induced tipping,” *Nonlinearity* **30**, 2185–2210 (2017).
- ⁷A. Vanselow, S. Wieczorek, and U. Feudel, “When very slow is too fast-collapse of a predator-prey system,” *Journal of theoretical biology* **479**, 64–72 (2019), doi:10.1016/j.jtbi.2019.07.008.
- ⁸P. Ritchie and J. Sieber, “Early-warning indicators for rate-induced tipping,” *Chaos* **26**, 093116 (2016), doi:10.1063/1.4963012.
- ⁹D. Faranda, F. M. E. Pons, E. Giachino, S. Vaienti, and B. Dubrulle, “Early warnings indicators of financial crises via auto regressive moving average models,”

- Communications in Nonlinear Science and Numerical Simulation **29**, 233–239 (2015), doi:10.1016/j.cnsns.2015.05.002.
- ¹⁰G. Nevo, N. Vercauteren, A. Kaiser, B. Dubrulle, and D. Faranda, “Statistical-mechanical approach to study the hydrodynamic stability of the stably stratified atmospheric boundary layer,” *Phys. Rev. Fluids* **2**, 084603 (2017), doi:10.1103/PhysRevFluids.2.084603.
- ¹¹A. Kaiser, D. Faranda, S. Krumscheid, D. Belusic, and N. Vercauteren, “Detecting regime transitions of the nocturnal and polar near-surface temperature inversion,” *Journal of the Atmospheric Sciences, AMS* **77**, 2921–2940 (2020), doi:10.1175/JAS-D-19-0287.1.
- ¹²D. Faranda and D. Defrance, “A wavelet-based approach to detect climate change on the coherent and turbulent component of the atmospheric circulations,” *Earth Syst. Dynam.* **7**, 517–523 (2016), doi:10.5194/esd-7-517-2016.
- ¹³D. Faranda, B. Dubrulle, and F. M. E. Pons, “Statistical early-warning indicators based on autoregressive moving-average models,” *Journal of Physics A: Mathematical and Theoretical* **47**, 252001 (2014), doi:10.1088/1751-8113/47/25/252001.
- ¹⁴H. Alkhayuon, P. Ashwin, L. C. Jackson, C. Quinn, and R. A. Wood, “Basin bifurcations, oscillatory instability and rate-induced thresholds for atlantic meridional overturning circulation in a global oceanic box model,” *Proc. R. Soc. A* **475** (2019), doi:10.1098/rspa.2019.0051.
- ¹⁵R. A. Wood, J. M. Rodriguez, R. S. Smith, L. C. Jackson, and E. Hawkins, “Observable, low-order dynamical controls on thresholds of the atlantic meridional overturning circulation,” *Climate Dynamics* **53**, 6815–6834 (2019), doi:10.1007/s00382-019-04956-1.
- ¹⁶V. Masson-Delmotte, P. Zhai, A. Pirani, S. Connors, C. Péan, S. Berger, N. Caud, Y. Chen, L. Goldfarb, M. Gomis, M. Huang, K. Leitzell, E. Lonnoy, J. Matthews, T. Maycock, T. Waterfield, O. Yelekçi, R. Yu, and B. Z. (eds.), “Ipcc 2021: Climate change 2021: The physical science basis. contribution of working group i to the sixth assessment report of the intergovernmental panel on climate change,” Cambridge University Press (2021).
- ¹⁷W. Weijer, W. Cheng, S. S. Drijfhout, A. Federov, A. Hu, and L. C. Jackson, “Stability of the atlantic meridional overturning circulation: A review and synthesis,” *Journal of Geophysical Research: Oceans* **124**, 5336–5375 (2019), doi:10.1029/2019JC015083.
- ¹⁸M. Hofmann and S. Rahmsdorf, “On the stability of the atlantic meridional overturning circulation,” *PNAS* **106**, 20584–2058 (2009), doi:10.1073/pnas.201798911.

- ¹⁹W. Liu, S.-P. Xie, Z. Liu, and J. Zhu, “Overlooked possibility of a collapsed atlantic meridional overturning circulation in warming climate,” *Science Advances* **3** (2017), doi:10.1126/sciadv.1601666.
- ²⁰S. E. Huisman, M. den Toom, H. A. Dijkstra, and S. Drijfhout, “An indicator of the multiple equilibria regime of the atlantic meridional overturning circulation,” *J. Phys. Oceanography* **40**, 551–567 (2010).
- ²¹W. Liu, Z. Liu, and E. C. Brady, “Why is the amoc monostable in coupled general circulation models?” *J. Clim* **27**, 2427–2443 (2014).
- ²²E. Hawkins, R. Smith, L. Allison, J. Gregory, T. Woollings, H. Pohlmann, and B. de Cuevas, “Bistability of the atlantic overturning circulation in a global climate model and links to ocean freshwater transport,” *Geophys. Res. Lett.* **38**, L10605 (2011).
- ²³N. Boers, “Observation-based early-warning signals for a collapse of the Atlantic Meridional Overturning Circulation,” *Nature Climate Change* **11**, 680–688 (2021).
- ²⁴J. Lohman and P. D. Ditlevsen, “Risk of tipping the overturning circulation due to increasing rates of ice melt,” *PNAS* **118** (2021), doi:10.1073/pnas.201798911.
- ²⁵G. Danabasoglu, “Ncar cesm2 model output prepared for cmip6 cmip,” (2019).
- ²⁶K. J. Preacher and E. C. Merkle, “The problem of model selection uncertainty in structural equation modeling,” *Psychological Methods* **17**, 1–14 (2012), doi:10.1037/a0026805.
- ²⁷R. J. Hyndman and Y. Khandakar, “Automatic time series forecasting: The forecast package for R,” *Journal of Statistical Software* **27** (2008).
- ²⁸G. Madan, J. H. LaCasce, A. Gjermundsen, and S. Iversen, “Weakening of the atlantic meridional overturning circulation under extreme climate change.” (2022), (In prep.).
- ²⁹N. P. Fofonoff and R. Millard Jr, “Algorithms for the computation of fundamental properties of seawater.” (1983).
- ³⁰T. M. Lenton, V. N. Livina, V. D. Dakos, E. H. van Nes, and M. Scheffer, “Early warning of climate tipping points from critical slowing down: comparing methods to improve robustness,” *Phil. Trans. R. Soc. A* **370**, 1185–1204 (2012).
- ³¹V. Dakos, S. R. Carpenter, W. A. Brock, A. M. Ellison, V. Guttal, A. R. Ives, S. Kefi, V. Livina, D. A. Seekell, E. H. van Nes, and M. Scheffer, “Methods for detecting early warnings of critical transitions in time series illustrated using simulated ecological data,” *PLoS ONE* **7**, e41010 (2012), doi:10.1098/rsta.2011.0304.

³²P. D. Ritche, J. J. Clark, P. M. Cox, and C. Huntingford, “Overshooting tipping point thresholds in a changing climate,” *Nature* **592**, 517–523 (2021), doi:10.1038/s41586-021-03263-2.

³³V. Laitinen, V. Dakos, and L. Lahti, “Probabilistic early warning signals,” *Ecology and Evolution* **11**, 14101–14114 (2021), doi:10.1002/ece3.8123.